Intersection of transient cell states with stable cell types in hippocampus

Jack A Olmstead[1,2,4]*, Lauren E King[3,4], Brenda L Bloodgood[3,4]*

[1] *Neurosciences Graduate Program*

[2] *Medical Scientist Training Program*

[3] *Department of Neurobiology, School of Biological Sciences*

[4] *UC San Diego School of Medicine, La Jolla, CA, United States*

* Corresponding Authors, jolmstea [at] health.ucsd.edu, blbloodgood [at] ucsd.edu

Abstract

The transcriptome of a brain cell encodes both its stable identity and its dynamic responses to environmental stimuli. While significant progress has been made in categorizing cell types within the brain, deciphering to what extent transcriptional identity and transcriptional state are related remains a major technical and conceptual challenge. Here, we present a single-nucleus RNA-sequencing atlas of the mouse hippocampus spanning physiological and pathological stimuli and multiple circadian phases, enabling unified analysis of activity-, circadian-, and cell-type-dependent transcriptional programs. Taxonomically assigned cell types are largely stable despite the induction of different activity states, with a notable exception in the dentate gyrus. Activity and circadian rhythm each drive robust, largely nonoverlapping transcriptional responses, with convergent regulation on genes involved in specific pathways, including endocannabinoid signaling, excitability, and chromatin remodeling. These results underscore the necessity of integrating cell-type taxonomy with transcriptional state to capture how diverse cell types respond to experience.

Introduction

Activity-dependent gene expression is a fundamental mechanism that neural cell types use to respond to experience and coordinate adaptive cellular responses. For canonical immediate-early genes (IEGs) such as *Fos*, *Egr1*, and *Npas4*, transcription begins to rise within minutes and peaks within an hour, highlighting the transient kinetics of these programs[1–6]. Large-scale transcriptomic atlases have provided precise molecular definitions of cell types in the brain[7,8], but interpretation of IEG expression within these foundational datasets has been fraught with known artifacts produced during cell capture, a process which itself induces IEGs[9,10]. A concerted effort is therefore necessary to characterize the intersection of activity states with a standardized taxonomy of cell types.

The hippocampus is a central structure for learning and episodic memory[11], and displays strong cell-type-specific network activity patterns during exploration and rest[12–17]. Behavioral states that drive plasticity—such as exploration during arousal and sharp-wave ripples during rest or sleep—predominate at different points in the circadian cycle, positioning the hippocampus as a model system for developing conceptual approaches to the integration of transcriptomic cell types and multidimensional cell states. Prior bulk RNA-seq studies in mice have shown circadian cycling of clock genes in the hippocampus[18,19], but no single-cell data exist to determine how neurons and glia engage these programs. Circadian phase influences excitability[20–23], seizure susceptibility[24,25], and memory performance[18,26], making the interaction between activity-dependent and circadian-dependent transcription biologically important, yet poorly characterized. To date, transcriptional rhythms across the circadian cycle have not been described in the hippocampus using single-cell RNA-seq approaches, leaving open how different cell types entrain their gene expression to this important biological variable.

In this study, we leverage state-of-the-art cell-type resources and a multifactorial experimental design to create an atlas of hippocampal cell states across activity conditions and circadian timepoints, which we call the Activity and Circadian

Transcriptomes Dependent on Physiological and Pathological activity (ACT-DEPP) dataset. With this resource, we show that enriched-environment (EE)- and seizure-induced neuronal activity engage qualitatively different transcriptomic programs within all cell types of the hippocampus. We find that within the Allen Brain Cell taxonomy of cell types, there is a collapse of cell type and activity state into a unitary identity among a subset of dentate granule cells. We describe a novel suite of marker genes that are transiently induced by activity in subpopulations of excitatory, inhibitory, and glial cells in the hippocampus. We report a gradient of IEG induction along the dorsal-ventral axis of CA1 in response to EE exposure. Finally, we show here that circadian rhythm coordinates widespread transcriptomic programs in both hippocampal neurons and glia at baseline. By comparing EE exposure to baseline states across the diurnal cycle, we systematically describe how activity- and circadian-dependent transcriptional programs intersect within hippocampal cell types and show that these variables influence endocannabinoid signaling, cell excitability, and chromatin remodeling.

By integrating transcriptional signatures of activity and circadian time into a taxonomy of cell types within the ACT-DEPP dataset, we provide both a conceptual framework for understanding state-dependent gene regulation and a resource for probing how activity patterns shape hippocampal plasticity across the circadian cycle.

Results

Generation of the ACT-DEPP dataset

Single-nucleus RNA sequencing (snRNA-seq) using SPLiT-seq[27] was performed on hippocampi from animals exposed to a standard environment (SE); an enriched environment (EE) for 30 minutes or 6 hours; or kainic acid-induced seizures (KA) for 30 minutes or 6 hours. The resulting dataset includes 93,066 nuclei from 48 biological replicates, capturing gene expression in baseline, physiological, and pathological activity conditions across circadian timepoints (**Fig. 1A-B, Supp. Fig. 1**).

79 Quality-controlled nuclei were annotated using MapMyCells and integrated with the Allen
80 Brain Cell (ABC) taxonomy, assigning each nucleus to hierarchical ranks of Class >
81 Subclass > Supertype > Cluster (**Fig. 1C inset;** ref [7]). Note: the Subclass rank generally
82 corresponds to conventionally understood cell types within the hippocampus, e.g.,
83 dentate granule cells, CA1, PV-expressing basket cells, etc. The UMAP embedding
84 recapitulated relations of canonical hippocampal cell populations at the Subclass level
85 (**Fig. 1C**), with additional clear transcriptional distinctions for both KA and EE conditions
86 within neuronal and glial Subclasses (**Fig. 1D**).

87 To confirm that cell-type annotation was independent of activity-induced transcriptional
88 states, a set of known activity-regulated genes[2] (ARGs) were removed, and annotations
89 were remapped. Cell-type re-annotations at the Class and Subclass rank were highly
90 stable (**Fig. 1E**-**F**), with minimal reassignment even at the lower ABC taxonomic ranks of
91 Subclass and Cluster (**Fig. 1G-H**). The ACT-DEPP dataset thus robustly registers
92 hippocampal cell types to the ABC taxonomy and reliably distinguishes transcriptional
93 states driven by physiological and pathological stimuli.

Figure 1

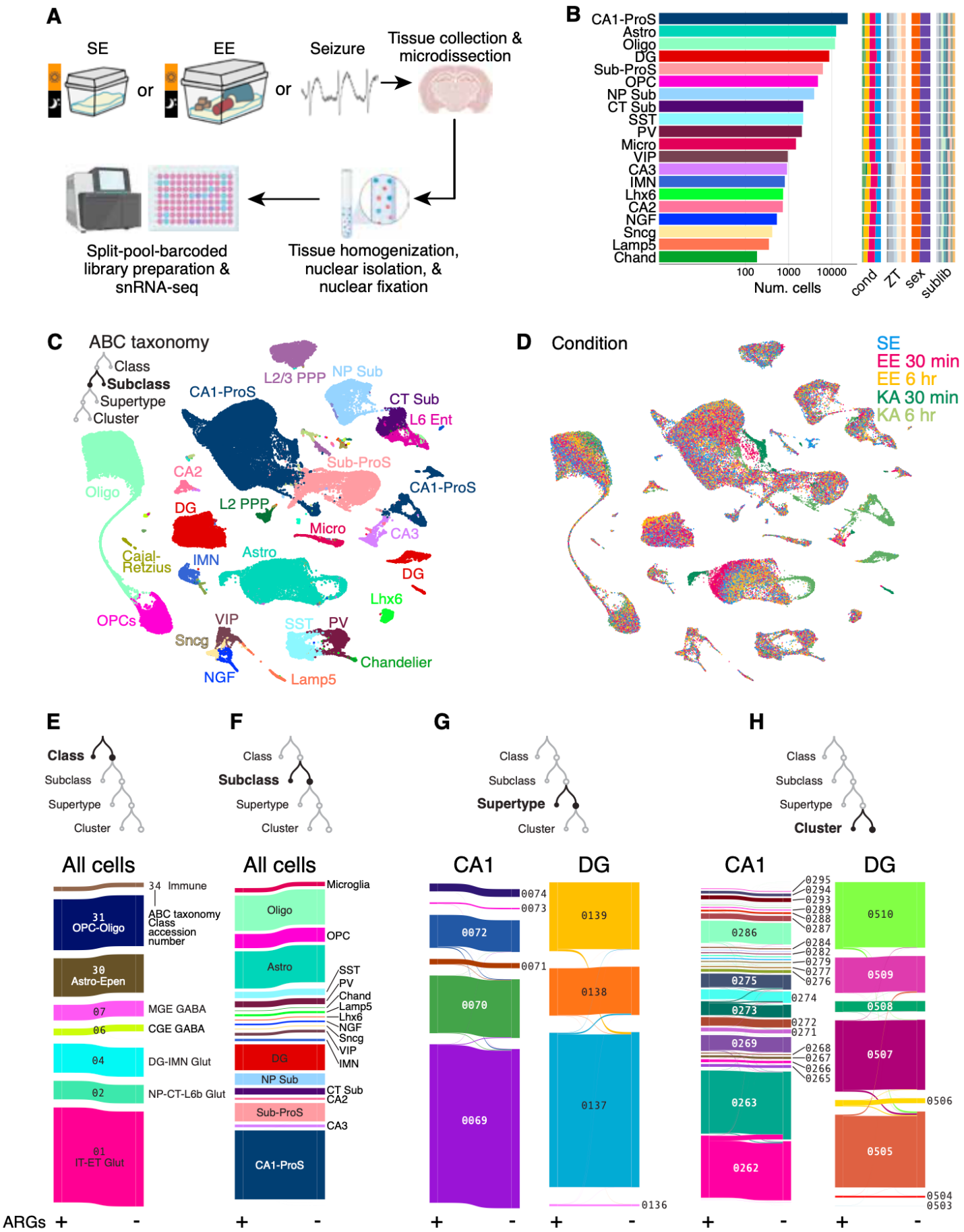
A
SE
EE
Seizure
Tissue collection & microdissection
or
or
Split-pool-barcoded library preparation & snRNA-seq
Tissue homogenization, nuclear isolation, & nuclear fixation
B
CA1-ProS
Astro
Oligo
DG
Sub-ProS
OPC
NP Sub
CT Sub
SST
PV
Micro
VIP
CA3
IMN
Lhx6
CA2
NGF
Sncg
Lamp5
Chand
100
1000
10000
Num. cells
cond
ZT
sex
sublib
C
ABC taxonomy
Class
Subclass
Supertype
Cluster
L2/3 PPP
NP Sub
CA1-ProS
CT Sub
L6 Ent
Sub-ProS
CA2
Oligo
CA1-ProS
DG
L2 PPP
Micro
CA3
Cajal-Retzius
IMN
Astro
DG
Lhx6
OPCs
VIP
SST
PV
Sncg
Chandelier
NGF
Lamp5
D
Condition
SE
EE 30 min
EE 6 hr
KA 30 min
KA 6 hr
E
Class
Subclass
Supertype
Cluster
All cells
34 Immune
31 OPC-Oligo
ABC taxonomy Class accession number
30 Astro-Epen
07 MGE GABA
06 CGE GABA
04 DG-IMN Glut
02 NP-CT-L6b Glut
01 IT-ET Glut
F
Class
Subclass
Supertype
Cluster
All cells
Microglia
Oligo
OPC
Astro
SST
PV
Chand
Lamp5
Lhx6
NGF
Sncg
VIP
IMN
DG
NP Sub
CT Sub
CA2
Sub-ProS
CA3
CA1-ProS
G
Class
Subclass
Supertype
Cluster
CA1
DG
0074
0073
0072
0071
0070
0069
0139
0138
0137
0136
H
Class
Subclass
Supertype
Cluster
CA1
DG
0295
0294
0293
0289
0288
0287
0286
0284
0282
0279
0277
0276
0275
0274
0273
0272
0271
0269
0268
0267
0266
0265
0263
0262
0510
0509
0508
0507
0506
0505
0504
0503
ARGs
+
-

Figure 1. Generation of the ACT-DEPP dataset.
(A) Experimental schematic of generation of the ACT-DEPP dataset.
(B) Distribution of nuclei number, experimental conditions, and sample metadata among major subclasses. Some neocortical and subiculum Subclasses appearing in Figure 1D have been omitted from this panel, as they were not analyzed in any further downstream analyses.
(C) UMAP embedding of ACT-DEPP nuclei colored by subclass. Inset: Single-nucleus transcriptomes were mapped to the Allen Brain Cell (ABC) whole-brain atlas, which assigns cells in a hierarchical taxonomy to one class, subclass, supertype, and cluster.
(D) As in (C), but colored by activity condition.
(E-H) Sankey flow diagrams showing changes in ABC-taxon identity for nuclei before (+) and after (-) removing ARGs from single-nucleus transcriptomes. (G) and (H) show the effect at lower ABC taxa for the two largest neuronal subclasses, CA1 and DG.
CA1-ProS, cornu ammonis 1-prosubiculum; L2/3 PPP, layer 2/3 pre-, pro-, parasubiculum; NP Sub, near-projecting subiculum; CT Sub, corticothalamic subiculum; L6 Ent, layer 6 entorhinal; DG, dentate gyrus granule cells; Sub-ProS, Subiculum-prosubiculum; Micro, microglia; Astro, astroglia; Oligo, oligodendrocyte; OPC, oligodendrocyte precursor cells; Epen, ependymal cell; NGF, neurogliaform cell; IMN, DG immature neuron; SST, GABAergic somatostatin-expressing interneuron; PV, GABAergic parvalbumin-expressing interneuron; GABAergic vasopressin internal peptide-expressing interneuron; Sncg, GABAergic Sncg-expressing interneuron; Lhx6, GABAergic Lhx6-expressing interneuron

The activity-dependent transcriptome is stimulus-specific and obscures cell identity in DG

Seizures have been used extensively to study ARG expression in the past, but direct comparisons to naturalistic stimuli are limited[28,29]. Moreover, the near-complete segregation of KA populations within some Subclasses in our uniform manifold approximation and projection (UMAP) plots led us to hypothesize that seizures constitute a categorically different transcriptional state from physiological manipulations. We therefore analyzed differentially expressed genes (DEGs) in CA1 and DG, the most abundant excitatory neuron Subclasses in our samples, at 30 minutes and 6 hours. KA induced an order of magnitude more DEGs than EE at both time points. Approximately one-third of EE-induced DEGs at 30 minutes were distinct from those induced by KA (**Fig. 2A**). At 6 hours, CA1 responses were fully shared between EE and KA, while DG maintained a unique DEG set specific to EE (**Fig. 2B**). Thus, novel experiences and seizures trigger categorically distinct transcriptional responses—with respect to both magnitude and specific genes—in these hippocampal subregions.

129 To look more closely at the effects of activity on different excitatory-neuron populations,
130 we re-embedded UMAPs and color-coded nuclei by condition or Subclass/Supertype
131 (**Fig. 2C**). Supertypes were clearly segregated within Subclass clusters, and strikingly,
132 distinct Supertypes emerged as seizure-specific populations. This effect was particularly
133 pronounced in DG, identified by its dramatically altered Supertype distributions between
134 activity conditions (**Fig. 2D**). In DG, nearly all KA cells clustered within Supertype 138-3,
135 with notable dissociation into Clusters 508-3 (KA 30m; green) and 509-4 (KA 6hr; purple,
136 **Fig. 2E**). Analysis of Cluster-defining genes revealed six marker genes strongly
137 associated with seizure timing and cluster identity (**Fig. 2F-G**): *Egr2, Egr4, Cenpa,*
138 *Bhlhe41, Lct, Npy*, the latter four not characterized as canonical ARGs. Thus, Supertype
139 DG 138-3 labels recently active granule cells, with additional discrimination of early and
140 late transcriptional responses to activity at the Cluster level. This would likely not be
141 detectable without both EE and KA conditions, given the sparsity of DG activation during
142 naturalistic activity[30–34].

Figure 2

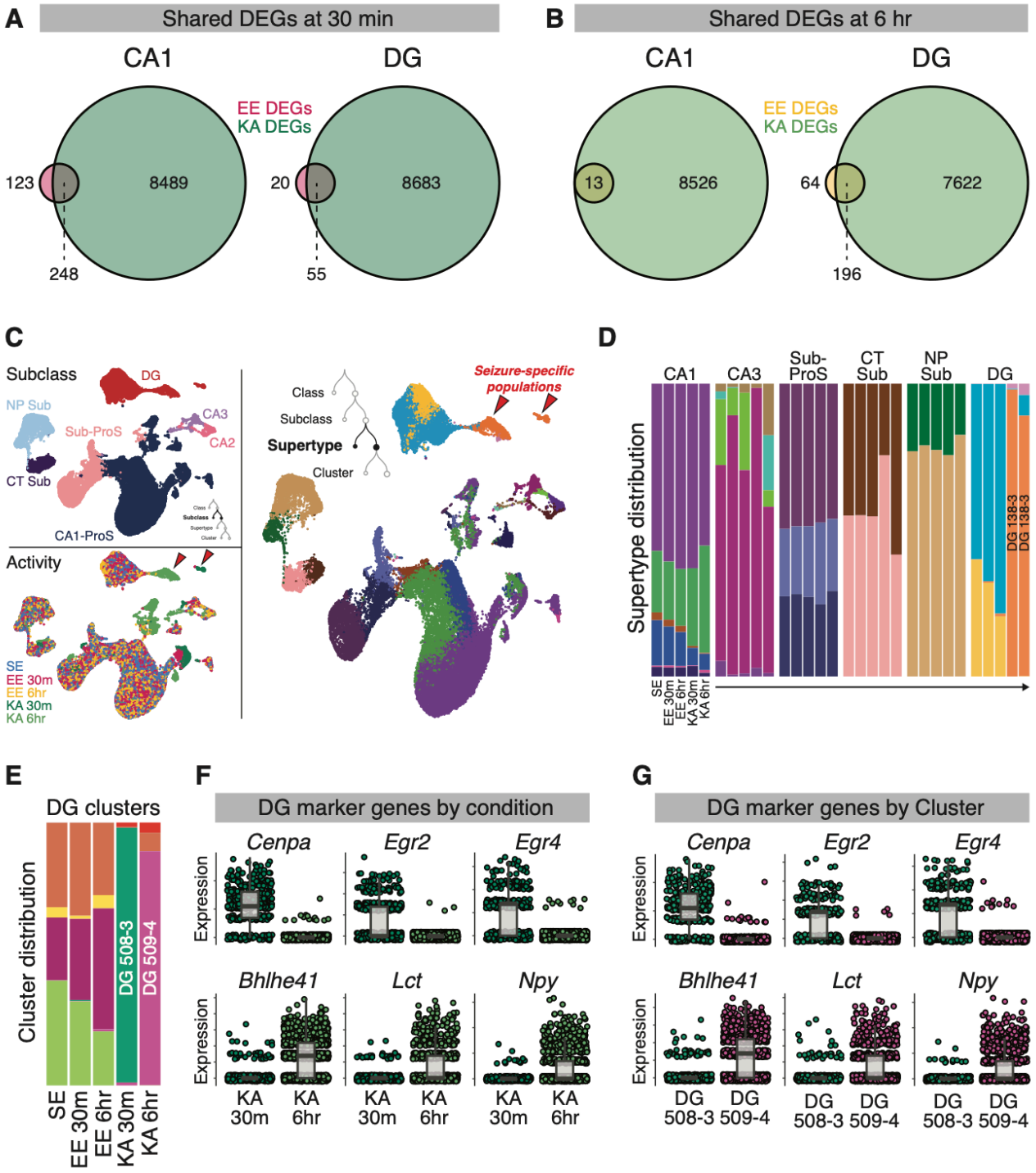
A
Shared DEGs at 30 min
CA1
DG
EE DEGs
KA DEGs
123
8489
248
20
8683
55
B
Shared DEGs at 6 hr
CA1
DG
EE DEGs
KA DEGs
13
8526
64
7622
196
C
Subclass
DG
NP Sub
CA3
Sub-ProS
CA2
CT Sub
CA1-ProS
Activity
SE
EE 30m
EE 6hr
KA 30m
KA 6hr
Class
Subclass
Supertype
Cluster
Seizure-specific populations
D
CA1
CA3
Sub-ProS
CT Sub
NP Sub
DG
Supertype distribution
DG 138-3
DG 138-3
SE
EE 30m
EE 6hr
KA 30m
KA 6hr
E
DG clusters
Cluster distribution
DG 508-3
DG 509-4
SE
EE 30m
EE 6hr
KA 30m
KA 6hr
F
DG marker genes by condition
Cenpa
Egr2
Egr4
Bhlhe41
Lct
Npy
Expression
KA 30m
KA 6hr
G
DG marker genes by Cluster
Cenpa
Egr2
Egr4
Bhlhe41
Lct
Npy
Expression
DG 508-3
DG 509-4

143 **Figure 2. The activity-dependent transcriptome is stimulus-specific and obscures cell**
144 **identity in DG.**
145 (A-B) Venn diagrams of shared DEGs between KA or EE vs SE at 30 min (A) or 6 hr (B) in CA1
146 (n_{EE30m} = 3329 nuclei, n_{SE} = 1907 nuclei, n_{KA30m} = 354 nuclei) and DG (n_{EE30m} = 7119 nuclei, n_{SE} =
147 6754 nuclei, n_{KA30m} = 961 nuclei). DEGs were defined as genes with absolute log2(FC) > 1.5 and
148 FDR < 0.05 using pseudobulk expression (Methods).
149 (C) Re-embedded UMAPs of excitatory neuronal nuclei colored by Subclass (left, top), activity
150 condition (left, bottom), or Supertype (right). Cross-reference of the UMAPs reveals KA-specific
151 populations marked by red arrows.
152 (D) Distribution of Supertypes within each subclass across different conditions. Colors within
153 each column represent proportions of different Supertypes within the labeled Subclass.
154 (E) As in (D), but for DG Clusters only.
155 (F-G) Single-nucleus, SC-transformed expression (Hafemeister & Satija 2019) of marker genes
156 for DG Cluster identity, plotted by condition (F) or Cluster (G)

157 **Discovery of cell-type-specific ERGs induced by novel experience**

158 To understand how different cell populations respond to naturalistic activity, we
159 compared early-response gene (ERG) expression across major groups of hippocampal
160 Subclasses (DEGs were categorized as either ERGs or LRGs based on their peak-
161 expression timing; see Methods and ref [10]). Both excitatory and inhibitory neurons share
162 broad upregulation of canonical ERGs such as *AP1*-, *Egr*-, *Nr4a*-, and *Dusp*-family
163 genes, *Arc*, and *Npas4* across nearly all Subclasses examined (**Fig. 3A, E**); these genes
164 unsurprisingly exhibit some of the strongest induction genome-wide across nearly all
165 Subclasses, including astrocytes and microglia (**Fig. 3B, F, I**).

166 Next, we were interested in determining which upregulated ERGs exhibited specific
167 activity-dependent induction in one or a few Subclasses. We calculated a tau specificity
168 score previously developed for bulk RNA-seq count data[35] to filter for specific changes
169 in expression within EE 30 min vs SE across Subclasses (Methods). When doing so, we
170 observe that canonical ERGs have some of the lowest cell-type specificity (**Fig. 3C, G,**
171 **J**). Meanwhile, screening for high-tau ERGs reveals genes whose induction is specific to
172 one or a few related cell types. For example, *Hs3st2* and *Rcan2* are both genes whose
173 expression is (1) specific to spatially restricted subiculum Subclasses, (2) acutely
174 upregulated following activity, and (3) decaying to baseline expression at 6 hours (**Fig.**
175 **3D**). Likewise, *Tac1* is an exemplar activity-dependent marker gene among PV-

176 expressing GABAergic cells and *Crhbp* in medial-ganglionic-eminence-derived
177 interneurons broadly (**Fig. 3H**). Finally, we make special note of the astrocytes, surprising
178 in their robust Subclass-specific response to acute EE exposure (**Fig. 3I-J**). Among the
179 DEGs, *Map3k19* and *Slco1c1* stand out as genes highly specific to activated astrocytes
180 (**Fig. 3K**). Thus, comparison of activity-dependent ERG expression following novel
181 experience yields novel marker genes with highly cell-type-specific induction.

Figure 3

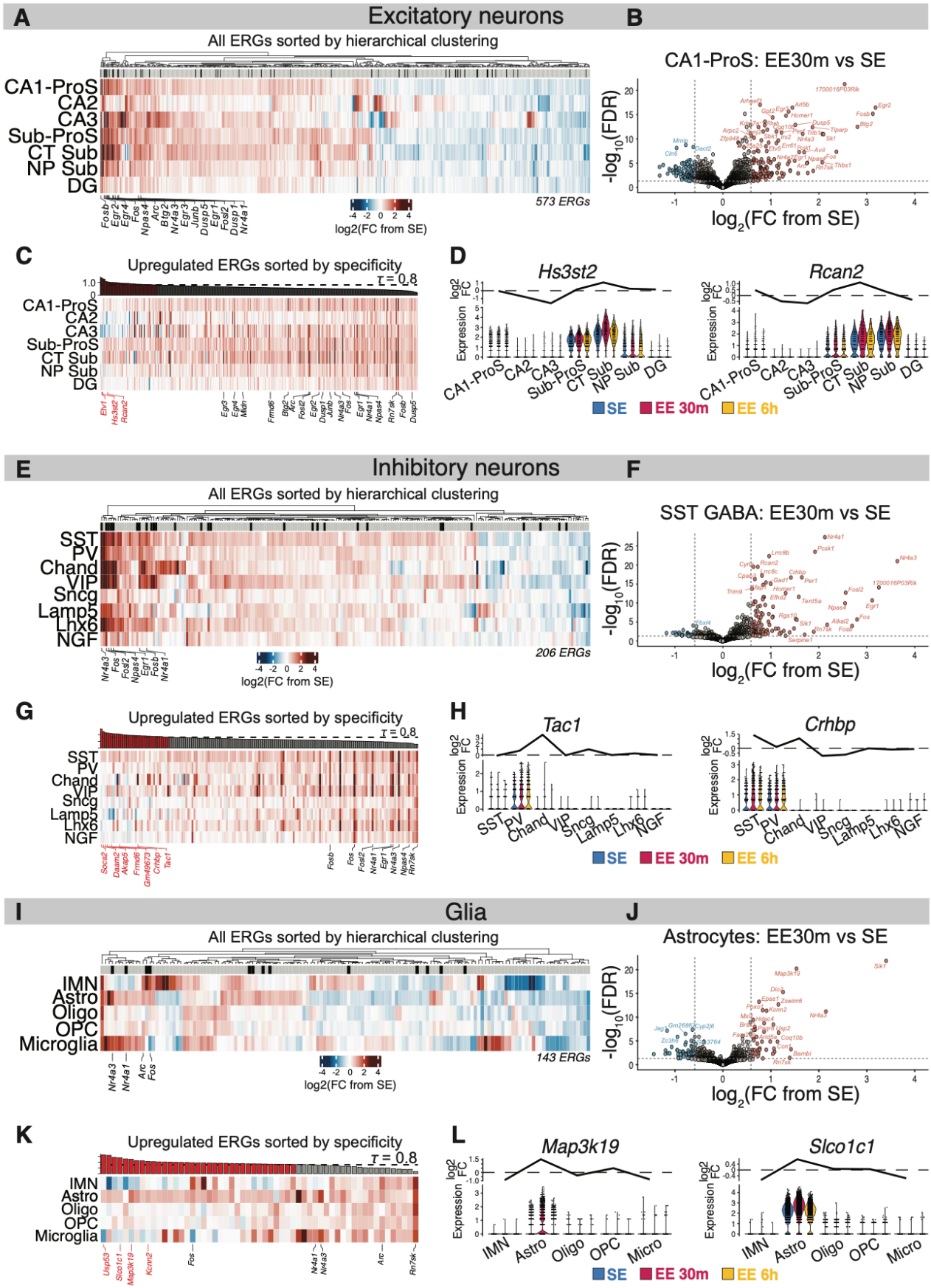
A
Excitatory neurons
B
All ERGs sorted by hierarchical clustering
CA1-ProS
CA2
CA3
Sub-ProS
CT Sub
NP Sub
DG
573 ERGs
log2(FC from SE)
CA1-ProS: EE30m vs SE
-log10(FDR)
log2(FC from SE)
C
Upregulated ERGs sorted by specificity
τ = 0.8
D
Hs3st2
Rcan2
Expression
SE
EE 30m
EE 6h
E
Inhibitory neurons
F
All ERGs sorted by hierarchical clustering
SST
PV
Chand
VIP
Sncg
Lamp5
Lhx6
NGF
206 ERGs
log2(FC from SE)
SST GABA: EE30m vs SE
-log10(FDR)
log2(FC from SE)
G
Upregulated ERGs sorted by specificity
τ = 0.8
H
Tac1
Crhbp
Expression
SE
EE 30m
EE 6h
I
Glia
J
All ERGs sorted by hierarchical clustering
IMN
Astro
Oligo
OPC
Microglia
143 ERGs
log2(FC from SE)
Astrocytes: EE30m vs SE
-log10(FDR)
log2(FC from SE)
K
Upregulated ERGs sorted by specificity
τ = 0.8
L
Map3k19
Slco1c1
Expression
SE
EE 30m
EE 6h

182 **Figure 3. Discovery of cell-type-specific ERGs induced by novel experience.**
183 (A) Change in expression in EE30m vs SE for all ERGs in excitatory neuronal subclasses; gene
184 columns are ordered by hierarchical clustering, and genes encoding transcription factors are
185 annotated with black ticks above heatmaps. For every Subclass, we performed pseudobulk DEG
186 analysis at EE 30 min vs SE and EE 6 hr vs SE. The heatmap contains all DEGs—ascertained
187 from any Subclass listed—that were classified as ERGs. ERGs are defined as DEGs whose fold-
188 change in EE vs SE was higher after 30 min instead of 6 hr (Methods).
189 (B) Volcano plot of DEGs in CA1-ProS nuclei at EE30m (n = 3329 nuclei) vs SE (n = 1907 nuclei).
190 (C) Heatmap of upregulated ERGs in excitatory neuronal Subclasses, ordered by Subclass-
191 specific induction (tau score; Methods). Canonical ERGs are annotated in black text, while novel
192 example Subclass-specific genes are annotated in red text.
193 (D) Violin plots of SC-transformed expression for example genes with high tau scores.
194 (E-H) as in (A-D) but for inhibitory neuronal subclasses.
195 (I-K) as in (A-D) but for immature neurons and glial subclasses.

196 **Distribution of IEG expression across CA1-ProS Supertypes**

197 Because CA1-ProS neurons were the largest Subclass in our dataset, we used the
198 opportunity to explore experience-induced activity responses within sub-populations of
199 these principal cells. First, we characterized activity in the entire population by adapting
200 a previously used method[10] to classify individual neurons as "active" or "inactive" based
201 on thresholded induction of immediate early genes (**Fig. 4A**; Methods). Crucially, our
202 library preparation captured only nuclear transcripts before they were exported to the
203 cytoplasm, increasing the likelihood that active cells are classified as such specifically in
204 response to the stimulus[3,9]. At baseline (SE), only 8% of cells were active. After 30
205 minutes of EE, activation increased to 33% of CA1 cells, then declined to 20% by 6
206 hours. KA seizure robustly activated nearly all cells at 30 minutes, decreasing to about
207 half at 6 hours, with a bimodal distribution possibly reflecting ongoing versus resolved
208 seizures[36] (**Fig. 4B**).

209 Transcriptionally defined Supertypes correspond to gradations of anatomically distinct
210 sub-populations of CA1 pyramidal neurons, evidenced by visualization within the ABC
211 MERFISH atlas[7] (**Fig. 4C**). We therefore hypothesized that we would observe differences
212 between CA1 Supertypes that may underlie functional specialization within the
213 hippocampus along anatomical axes[37,38]. We find that EE strongly activates Supertypes
214 69-1 and 70-2 compared to others—notable given the dorsal distribution of these

215 Supertypes within hippocampus (**Fig. 4C**) and the engagement of this part of the
216 hippocampus during exploration[39–41]. In contrast, KA seizure manipulations demonstrate
217 that all Supertypes are competent at inducing IEGs following 30 minutes of global
218 activity, although variation in active cells at 6 hours suggests differences in ongoing
219 neural activity, ongoing transcription, or mRNA export among CA1 Supertypes (**Fig. 4D-**
220 **E**).

221 Prior single-cell studies have analyzed IEG expression in different neuronal cell types,
222 including in the hippocampus, to discern whether there are IEG "modules," i.e. genes
223 that are co-induced together[8,10,29]. No such analyses have revealed any interpretable
224 structure of IEG activation. We sought to determine if the unprecedented cell-type
225 resolution among ABC taxa in our dataset would reveal patterns of IEG expression in
226 CA1 subpopulations that were aggregated in prior analyses. If a pattern to stimulus-
227 dependent IEG induction existed, it would emerge in recently active cells, appearing as
228 highly correlated expression modules among IEG subsets, with anti-correlation between
229 subsets. When we tested this hypothesis among active cells in our most abundant
230 Supertypes after 30 minutes of EE, we observed patterns of modest positive correlation
231 among nearly all canonical IEGs across all Supertypes (**Fig. 4F**). We therefore conclude
232 there is minimal evidence for structured or modular expression of IEGs within subsets of
233 CA1-ProS neurons.

Figure 4

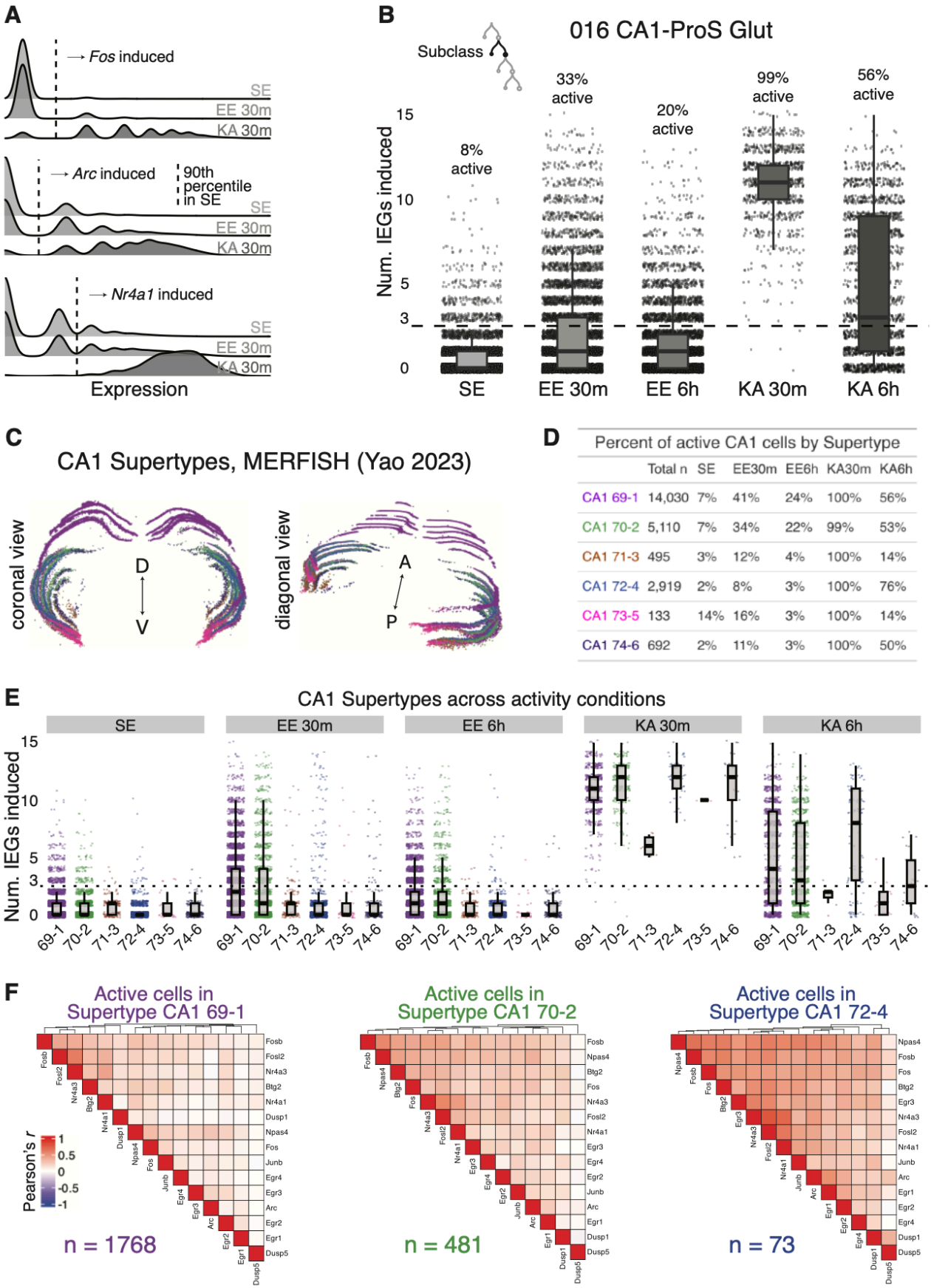

	Total n	SE	EE30m	EE6h	KA30m	KA6h
CA1 69-1	14,030	7%	41%	24%	100%	56%
CA1 70-2	5,110	7%	34%	22%	99%	53%
CA1 71-3	495	3%	12%	4%	100%	14%
CA1 72-4	2,919	2%	8%	3%	100%	76%
CA1 73-5	133	14%	16%	3%	100%	14%
CA1 74-6	692	2%	11%	3%	100%	50%

Figure 4. Distribution of IEG expression across CA1-ProS Supertypes.
(A) Example plots demonstrating IEG induction thresholds using *Fos*, *Arc*, and *Nr4a1*. For a given gene, the induction threshold was defined as the 90th percentile of expression among SE nuclei; thresholds are represented as dotted lines.
(B) Activation of single cells across activity conditions within CA1-ProS neurons. Active cells were defined as those that induced 3 or more IEGs, similar to the approach in Hrvatin et al. 2018 (Methods).
(C) 3-D plots of ABC MERFISH brain slices (published data from Yao et al. 2023) with only CA1-ProS Supertypes plotted.
(D-E) Activation percentages as in (B), de-aggregated by Supertype.
(F) Gene-gene correlation matrices for IEG expression within active cells at EE 30 min. Dendrograms represent hierarchical clustering of genes.

Circadian-dependent transcription among major hippocampal cell types in SE

Biological rhythms entrained to the diurnal light cycle are ancient cellular processes driven by transcription-translation feedback lopps that occur in many tissues, including the mouse hippocampus[23,42]. Yet, circadian cycling of transcription remains poorly understood outside the suprachiasmatic nucleus, with no single-cell studies characterizing the extent to which this occurs among different cell types in the hippocampus. We therefore sought to characterize transcriptional changes occurring at four Zeitgeber time points (ZTs) throughout the diurnal cycle under baseline conditions using our snRNA-seq approach, focusing on the four largest Subclasses to reduce noise. Canonical clock genes *Per1*, *Per2*, and *Cry2* peaked at ZT12 (start of the dark cycle), whereas *Clock* and *Bmal1* had opposite periodicity at ZT0 (**Fig. 5A**), aligning with previous hippocampal studies[18,19,23,43–47].

We next sought to characterize transcriptional changes taking place genome-wide using DGE analysis. When doing so, we capture the differential expression of canonical clock genes in every subclass tested (**Fig. 5B-E**, yellow annotations). We note again that *Per*-family expression peaks at ZT12 in every case but one. In addition to the *Per* family, its heterodimer partners *Cry1*, *Cry2*—as well as transcriptionally correlated Clock-gene regulators *Nr1d1*, and *Nr1d2*—peak at ZT12 in Subclasses where they are differentially expressed (**Fig. 5B-D**). Conversely, although we do not capture differential expression of *Clock* and *Bmal1* in every Subclass, their peak expression in such cases is not

266 concurrent with *Per*-, *Cry*-, or *Nr1d*-family peaks. These phase-shifted expression peaks
267 are functionally consistent with the canonical transcription-translation feedback loop
268 that undergirds circadian rhythms[48]. Thus, the ACT-DEPP dataset captures circadian
269 oscillations of transcription with high fidelity in multiple neuronal and glial cell types.

270 We next created UMAP embeddings of single-nucleus transcriptomes in circadian-DEG
271 space (2725 genes across all Subclasses) to determine whether there is a transcriptomic
272 structure tracking circadian time. We observe a clear separation of nuclei collected at
273 ZT12 in every Subclass examined, with additional gradations of other timepoints in some
274 cell types (**Fig. 5B-D**). High tau-specificity analysis confirms statistically what is visually
275 apparent: In all Subclasses, ZT12 is a unique circadian-transcriptomic state with broad
276 upregulation of many genes specifically at that time. Interestingly, in CA1-ProS cells, 12
277 of 17 of high-tau genes encoded lncRNAs, in contrast to DG granule cells (0/1),
278 astrocytes (4/13) and oligodendrocytes (4/40). This points to a unique recruitment of the
279 non-coding transcriptome in CA1-ProS neurons during this diurnal transition, the
280 functional significance of which is unclear. Finally, among previously characterized
281 ARGs[2] (ref [49] for *Adcy* genes), several of these varied throughout the circadian cycle,
282 suggesting that there may be an interaction between ZT and activity within the
283 hippocampus.

Figure 5

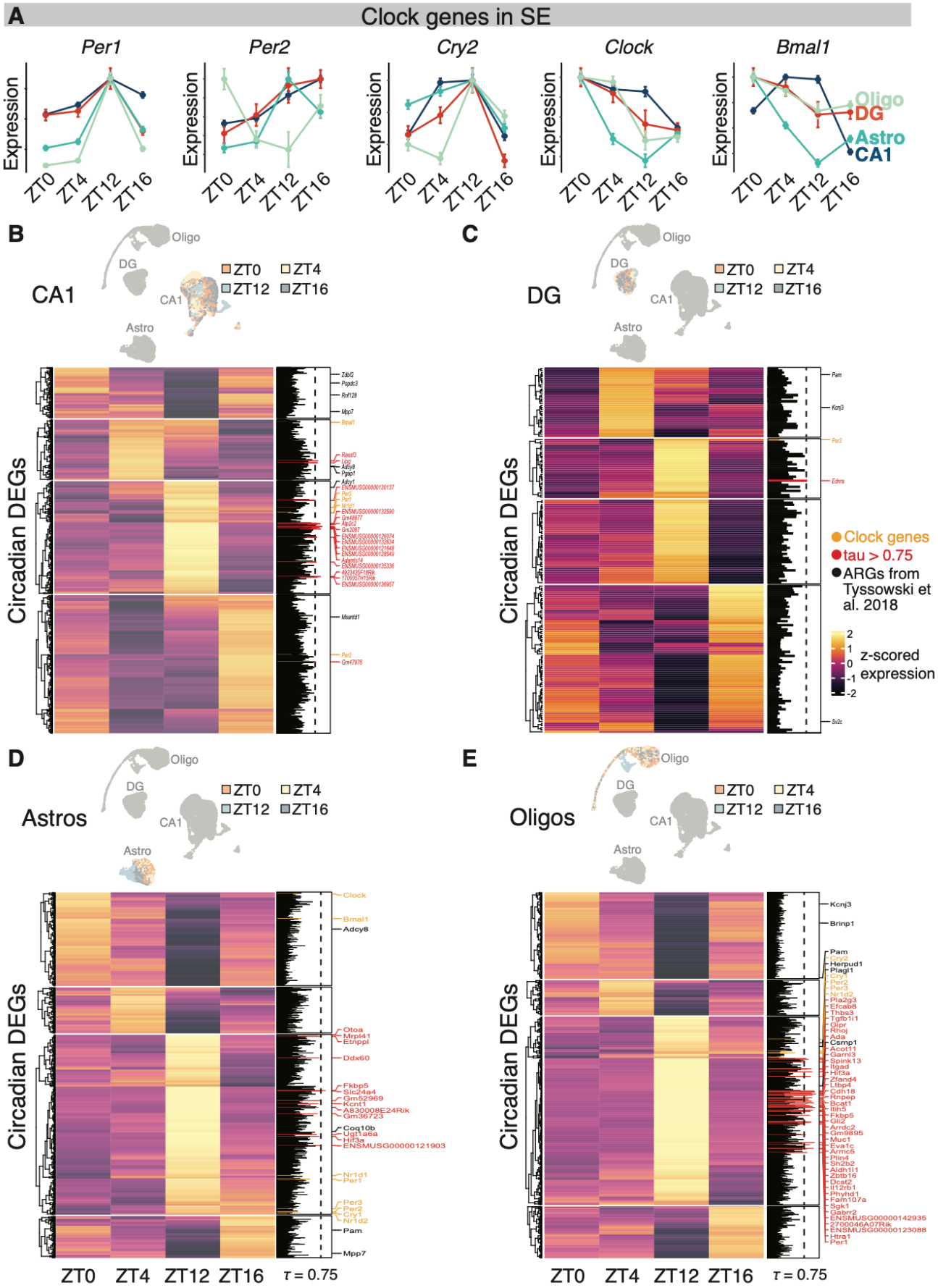
A
Clock genes in SE
Per1
Per2
Cry2
Clock
Bmal1
Expression
ZT0
ZT4
ZT12
ZT16
Oligo
DG
Astro
CA1
B
CA1
C
DG
D
Astros
E
Oligos
ZT0
ZT4
ZT12
ZT16
Circadian DEGs
Clock genes
tau > 0.75
ARGs from Tyssowski et al. 2018
z-scored expression
τ = 0.75

Figure 5. Circadian-dependent gene expression among major hippocampal cell types.
(A) Pseudobulk expression of canonical clock genes across the circadian period in SE. Error bars represent s.e.m.
(B-E) Above: UMAP embeddings of nuclei in circadian-DEG space, colored by ZT of collection (Methods). Below: Pseudobulk expression for circadian DEGs across the diurnal cycle. Clock genes (yellow), high-tau genes (red), and ARGs (black) are highlighted.

Interactions between activity- and circadian-dependent transcription in hippocampus

Previous studies have shown differences in canonical ARG expression at different times of day, although these studies could not make direct claims about stimulus-specific ARG induction due to their experimental design[18,18,19]. To directly test whether circadian time influences activity-dependent gene expression, we performed EE exposure at different ZTs. We hypothesized, based on these prior studies, that ARG induction would vary in at least some cell types across circadian time; that is, fold-change in ARG expression in EE vs SE would not be constant across the circadian period. We restricted our initial analyses to IEG and clock gene sets used in **Figures 4** and **5**, respectively. Surprisingly, there were no significant ZT:Activity interactions for IEGs in any of the Subclasses tested (**Fig. 6A-D**). This was unexpected, given previous reports of circadian-dependent IEG expression at baseline and upstream signaling cascades using non-RNA-seq methods[43,49,50]. We nevertheless note strong IEG induction in CA1, irrespective of ZT, unlike other Subclasses.

Having established that the expression of clock genes varies substantially in baseline conditions (**Fig. 5A**), we hypothesized that, if present, activity-dependent induction of these genes would not be uniform across ZTs. Indeed, we find that not only are *Per1* and *Per2* inducible in response to EE exposure, but also that *Per1* exhibits a significant ZT:Activity interaction in all Subclasses except DG, with inducibility restricted to times excluding ZT12—notable because ZT12 corresponds to peak expression in SE (**Fig. 5A**). This observation can be interpreted as a “ceiling effect” of EE-induced expression mimicking the peak circadian expression.

313 Finally, we tested for ZT:Activity interaction genome-wide. Surprisingly, we only found a
314 small number of genes whose expression was significantly modulated by ZT:Activity
315 interaction, and these genes only appeared in the neuronal Subclasses (**Fig. 6I-J**).
316 Among the cell types tested, we observe 13 genes that have a statistically significant
317 interaction between ZT:EE exposure, none of which are canonical IEGs. Functional
318 annotation of these genes reveals that two are involved in endocannabinoid synthesis
319 (*Daglb, Napepld*), three in cell signaling or excitability (*Fcho2, Itpkb, Kcnn2*), and four in
320 chromatin remodeling or gene expression (*Cecr2, Zfp420, Zpf523*). We therefore
321 conclude that changes in gene expression following novel experience are relatively
322 constant across the circadian cycle, although special mechanisms may be in place to
323 selectively change induction mechanisms for genes which modulate endocannabinoid
324 synthesis and cell excitability within neurons of the hippocampus.

Figure 6

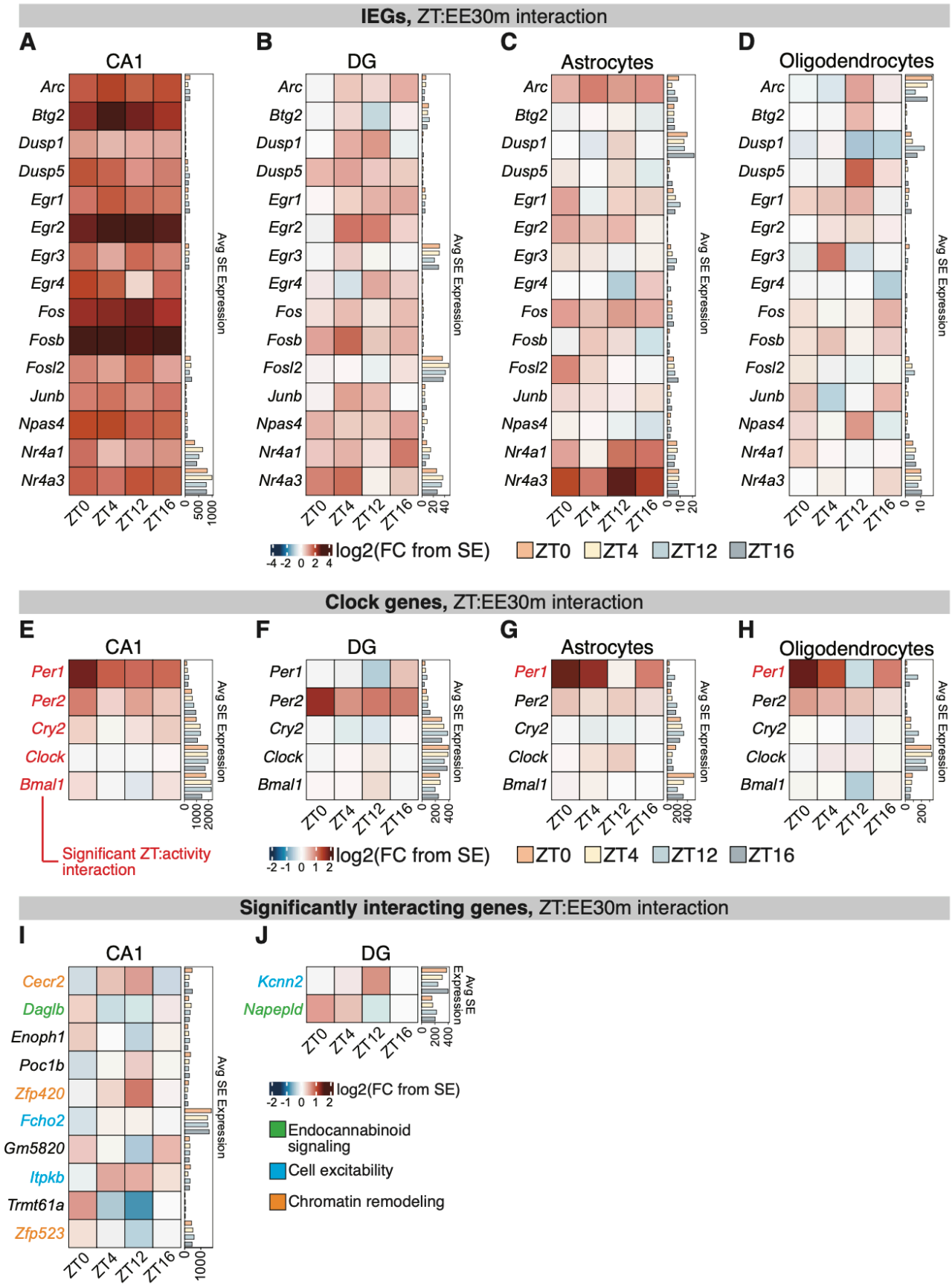
IEGs, ZT:EE30m interaction
A
CA1
B
DG
C
Astrocytes
D
Oligodendrocytes
Arc
Btg2
Dusp1
Dusp5
Egr1
Egr2
Egr3
Egr4
Fos
Fosb
Fosl2
Junb
Npas4
Nr4a1
Nr4a3
ZT0
ZT4
ZT12
ZT16
Avg SE Expression
log2(FC from SE)
-4 -2 0 2 4
ZT0
ZT4
ZT12
ZT16
Clock genes, ZT:EE30m interaction
E
CA1
F
DG
G
Astrocytes
H
Oligodendrocytes
Per1
Per2
Cry2
Clock
Bmal1
Avg SE Expression
Significant ZT:activity interaction
log2(FC from SE)
-2 -1 0 1 2
ZT0
ZT4
ZT12
ZT16
Significantly interacting genes, ZT:EE30m interaction
I
CA1
J
DG
Cecr2
Daglb
Enoph1
Poc1b
Zfp420
Fcho2
Gm5820
Itpkb
Trmt61a
Zfp523
Kcnn2
Napepld
Avg SE Expression
log2(FC from SE)
-2 -1 0 1 2
Endocannabinoid signaling
Cell excitability
Chromatin remodeling

Figure 6. Interactions between activity- and circadian-dependent transcription in the hippocampus.
(A-D) Expression change between EE30m vs SE for IEGs across the circadian period. Baseline pseudobulk expression for each gene at each ZT is plotted on the right.
(E-H) As in (A-D) but for canonical clock genes.
(I) Expression change between EE30m vs SE for genes with significant ZT:activity_condition interaction (Methods). Baseline pseudobulk expression for each gene at each ZT is plotted on the right.
(J) As in (I) but for DG. Note: astrocytes and oligodendrocytes had no significantly interacting genes between ZT and activity condition.

Discussion

The ACT-DEPP dataset is an atlas of single-nucleus transcriptomes from the hippocampus, capturing transcriptional responses to both physiological and pathological brain activity. The creation of this atlas accomplishes two goals: (1) mapping of experience-dependent gene expression in a high-resolution cell-type taxonomy, and (2) characterization of circadian-dependent transcriptional oscillations in both neurons and glia of the hippocampus. All cell types are registered to a gold-standard brain-wide taxonomy, providing rich annotation that we leverage to demonstrate that stimulus-responsive cell states are embedded within broader cell-type identities, such as hippocampal sub-region (**Fig. 3**) and anatomical location (**Fig. 4**), with DG serving as an exception to this rule (**Fig. 2**). We identify the light-to-dark transition as a key inflection point for diurnal gene regulation in the hippocampus (**Fig. 5**) and show that activity-dependent induction does not vary widely across the circadian period (**Fig. 6**). We envision this resource as a roadmap for analyzing cell-type-specific, stimulus-responsive states in the brain using modern transcriptome-registration tools. More broadly, the ACT-DEPP dataset is a resource for understanding how physiological and pathological activity patterns drive experience-dependent transcriptional programs to support neural plasticity across the circadian cycle.

353 **Limitations**

354 We take care to point out a potential conceptual limitation of our study: Dissociating
355 neuronal gene expression driven by circadian phase from that driven by acute
356 locomotion is inherently challenging because the two are tightly coupled in behavior and
357 physiology. Locomotor activity co-occurs with changes in arousal, hormones, and
358 neuromodulator release, many of which independently influence transcription, while the
359 propensity for locomotor activity varies across the circadian cycle[23,51]. One argument that
360 favors the distinction we make between activity- and circadian-dependent expression is
361 that canonical IEGs do not overlap with circadian DEGs (**Fig. 5**), suggesting orthogonal
362 regulatory logic between activity programs and circadian programs. Second, in contrast
363 to neurons, glial transcription is less sensitive to rapid fluctuations in circuit activity and
364 more influenced by systemic cues, making their rhythmic gene expression less
365 confounded by locomotor events. Taken together, these observations support the
366 validity of interpreting our findings as reflecting both activity- and circadian-driven
367 transcriptional programs, rather than a single merged signal.

368 We also disclaim notable variance in cell number and read depth among a small number
369 of our biological replicates (**Supp. Fig. 2 and 3**). Although our pseudobulk approach
370 accounts for both of these factors by computing size factors for gene-count
371 normalization before performing DGE analysis, it is nevertheless likely that estimates of
372 variance are noisier in these conditions. However, for all of our DGE analyses, we set
373 DESeq2 gene-filtering parameters that would bias our analysis toward excluding genes
374 from DEG lists based on unacceptably high levels of within-condition variance for that
375 gene model. Pseudobulk DGE analysis has been shown to be the most robust against
376 Type I errors for single-cell data while performing the best in balancing Type II error
377 rate[52,53]. Thus, the results reported in this paper should be protected from unacceptably
378 high false-positive rates.

379 **Cell states and cell types**

380 Beyond our investigation of circadian transcription, our study has three main
381 contributions to our understanding of activity-dependent gene expression. First, we
382 extensively leverage registration of our dataset with the ABC atlas—a state-of-the-art
383 ontology of cell types in the mouse brain[7]—to query activity-dependent states among
384 high-resolution cell types. The ability to observe the effects of activity manipulations at
385 the Supertype and Cluster level allows us to infer activity distributions along functionally
386 relevant anatomical axes in the hippocampus (**Fig. 4**). Second, we distinguish several
387 candidate genes that are highly specific not only to cell types, but also activity states
388 (**Fig. 3**). These genes may serve as guideposts for the development of simpler next-
389 generation tools to study activity-dependent processes with cell-type granularity going
390 beyond IEG-based permanent labeling systems using *Fos, Arc, or Npas4*[54–57]—all of
391 which are broadly upregulated across multiple cell types in our data, including non-
392 neuronal cell types (**Fig. 3**). Such tools would have the advantage of being able to
393 permanently access task-specific ensembles within specific cell types without the need
394 for complex intersectional genetic strategies. Third, our descriptions of activity in
395 baseline and "ceiling" conditions such as seizure provide strong evidence for the
396 annotation of specific Supertypes and Clusters as highly temporally specific signatures
397 of recent activity (**Fig. 2**).

398 Within DG granule cells, we observed a collapse of cell type and activity state at the
399 supertype level (**Fig. 2**), and we also demonstrate that the Cluster rank in this population
400 further resolves activity states into both acute and subacute activity histories, on the
401 order of 30 minutes to 6 hours within our dataset (**Fig. 2E**). This example case in DG
402 begs the question: Does the annotation of activity state—or any other condition-specific
403 state, e.g. cellular manipulation or disease—at the Supertype or Cluster rank merit the
404 collapse of these taxa with closely related inactive populations within the ABC
405 taxonomy? More broadly, to what extent should reference atlases balance heterogeneity
406 of cell states with the classification of cell types? On the one hand, the development of
407 genetic tools to interrogate a particular Supertype or Cluster may produce unexpected

408 results if that taxon represents a distinct cell state not present, or overrepresented, within
409 an experimental dataset. On the other hand, it is easy to imagine how the annotation of
410 active DG cells, for example, through a simple compositional analysis of Supertypes or
411 Clusters would be useful for high-throughput readout of activity. It is our opinion that the
412 correlation of specific cell states with lower ranks in the ABC atlas is acceptable, as long
413 as these cell states are ascertained using robust experimental methods whose results
414 are clearly disclosed to the community.

415 **Circadian rhythm changes baseline gene expression in the hippocampus**

416 It has long been established that cells in the suprachiasmatic nucleus (SCN) use
417 transcription-translation feedback loops entrained to ambient-light sensation to keep a
418 "molecular clock" that tracks the diurnal cycle (Patton & Hastings 2018; Patton 2023).
419 However, there are few investigations of hippocampal circadian-dependent transcription
420 in the omics era, and no snRNA-seq studies that we are aware of. Therefore, we sought
421 to characterize how transcription changes in the hippocampus across the circadian
422 cycle using snRNA-seq. Our results extend previous work by confirming the presence of
423 clock-gene cycling in hippocampal neurons and glia across the circadian cycle. The
424 expression patterns of canonical clock genes we observe are consistent with earlier bulk
425 hippocampal studies[18,19,23,43], lending confidence that our sampling strategy captures
426 genuine circadian processes rather than stochastic variation. Importantly, we find that
427 ZT12 represents a distinct transcriptional inflection point across multiple cell types,
428 coinciding with the transition from the light to dark period. This time is behaviorally salient
429 for nocturnal animals such as mice, as locomotor activity begins to rise sharply before
430 and during the onset of darkness[23,46,51,58]. Our data therefore support the interpretation
431 that circadian gene expression in hippocampal cells is tightly coupled to this
432 environmental and behavioral transition.

433 The similarity of transcriptomic profiles at ZT16 and ZT0 further suggests that circadian-
434 driven transcription is concentrated within a narrow temporal window. Rather than a
435 gradual progression across the cycle, many genes appear to undergo sharp, temporally

436 restricted bursts of expression near the light–dark transition. This "bursty" model of
437 circadian regulation is consistent with prior reports of pulse-like transcription in single
438 cells[59–62] and may reflect a strategy by which hippocampal cells track salient transitions
439 without maintaining high levels of rhythmic transcription throughout the entire dark
440 period.

441 Among the cell types tested, we observed a striking specificity in circadian-dependent
442 transcription: oligodendrocytes, which exhibit relatively few activity-dependent DEGs
443 (**Fig. 3**), display the largest number of circadian DEGs. This dissociation underscores
444 that activity-dependent and circadian-dependent transcription represent partially non-
445 overlapping regulatory axes. For oligodendrocytes, the high number of circadian DEGs
446 suggests that diurnal regulation may play a dominant role in processes such as myelin
447 turnover or sheath maintenance, at least during the developmental period tested
448 (approximately P28 mice). In contrast, neuronal populations such as CA1 exhibit fewer
449 circadian DEGs overall, with enrichment of lncRNAs at ZT12 compared to other cell
450 types, hinting at separate mechanisms of regulatory control. Together, these results
451 suggest that circadian transcription exerts heterogeneous but highly structured influence
452 across hippocampal cell types.

453 **Circadian cycle has limited effect on activity-dependent transcription**

454 We found no circadian differences in IEG induction (**Fig. 6A–D**), despite expecting higher
455 expression in the dark period due to increased locomotor activity[51], state-dependent
456 hippocampal network events such as sharp-wave ripples during rest[14], and prior reports
457 of circadian oscillations in cAMP, MAPK, and CREB signaling[49,51,63,64]. Instead, IEGs were
458 induced uniformly across the diurnal cycle in both neuronal and glial populations,
459 exemplified by CA1 cells (**Fig. 6**). Prior work reported dark-phase upregulation of IEGs
460 in rats under chronic EE[65] or in cortex at ZT20[50], but those studies differ in species, brain
461 region, EE paradigm, stimulus, timing, and bulk vs. snRNA-seq, making direct
462 comparison to our results inappropriate.

463 It has been previously shown that *Per* genes are inducible in the hippocampus in
464 response to circuit activity[18,19,47], a finding that we recapitulate after 30 minutes of EE.
465 This finding, in conjunction with *Per*'s circadian oscillations in the absence of activity,
466 raises important conceptual questions. What does it mean for there to be circadian-
467 dependent expression when these genes are also induced by activity? We observe that
468 at the highest peaks of EE-responsive induction, *Per* expression is comparable to its
469 circadian peak. One speculation that could explain this phenomenon is that in the
470 absence of activity, daily peaks in *Per* induction "guarantee" a dose of permissive
471 regulatory-element access for PER-CRY target genes which would otherwise not be
472 transcribed but are nevertheless necessary for cell function; activity-dependent *Per*
473 expression would act as an adjuvant to predictable circadian bursts, possibly at genes
474 important for cellular adaptations to circuit activity. Clearly, additional studies are
475 necessary to understand the multifactorial causes and functional consequences of *Per*
476 expression.

477 When testing for ZT:activity interaction genes, only 13 DEGs were found, all in neuronal
478 subclasses. The functional classes of these DEGs suggest that there is a special role for
479 fluctuations in intercellular endocannabinoid signaling throughout the circadian cycle, an
480 enticing idea that may be relevant for neurological phenotypes. For example, despite the
481 untold number of molecular etiologies for different epilepsies, circadian rhythms to
482 seizure attacks are common in drug-resistant epilepsy, occurring in approximately 90%
483 of patients[25]. This observation implies that there are circadian changes taking place in
484 the brain that are not themselves pathogenic, but may affect seizure threshold across
485 the diurnal cycle. In summary, our examination of the intersection of activity- and
486 circadian-dependent gene expression is an important first step toward understanding
487 the circadian transcriptome in the hippocampus, as it may canalize certain disease
488 phenotypes.

Author contributions

Jack A Olmstead: Conceptualization, Investigation, Methodology, Data curation, Formal analysis, Software, Visualization, Writing – original draft, Writing – review and editing

Lauren E King: Investigation, Writing – review and editing

Brenda L Bloodgood: Conceptualization, Supervision, Project administration, Funding acquisition, Writing – original draft, Writing – review and editing

Acknowledgements

We thank members of the Bloodgood lab and Dhanajay Bambah-Mukku for continuous discussion and feedback about experimental results and data analysis. We are indebted to Eric Halgren for providing computing resources. We thank Elizabeth Chamiec-Case and Lauren Valdez for their assistance with experimental troubleshooting. We kindly acknowledge the detailed experimental and analytic support provided by Brian Davis, Sam You, and Daniel Diaz of Parse Biosciences. This work was supported by funding awarded to BLB by the National Institute of Neurological Disorders and Stroke (R01 NS111162) and to the UC San Diego Medical Scientist Training Program (T32 GM154642). This publication includes data generated at the UC San Diego IGM Genomics Center utilizing an Illumina NovaSeq X Plus that was purchased with funding from a National Institutes of Health SIG grant (#S10 OD026929).

The authors declare no competing interests.

Materials and Methods

Animals

Animal experiments were approved by the University of California San Diego Institutional Animal Care and Use Committee and followed guidelines according to the National Institutes of Health's *Guide for the Care and Use of Laboratory Animals.* All experiments used wild-type C57BL6/J mice from The Jackson Laboratory (JAX#000664). Mice were

516 approximately four weeks old, with balanced proportions of males and females
517 distributed across control and experimental groups (**Supp. Table 1**).

518 **Experimental procedures**

519 *Standard environment and circadian timepoints*

520 Mice were group-housed in a vivarium on a 12-hour light/dark cycle and provided food
521 *ad libitum*. To avoid non-experimental stimulation artifacts resulting from cage handling
522 or transport, mice were transported from the vivarium to the standard environment (SE)
523 at least 18 hours before experiments. The SE consisted of a plywood box paneled with
524 sound-dampening foam, air-circulation fans, and LED lights whose power was controlled
525 by a timer mimicking the vivarium's light/dark cycle. Circadian timepoints were
526 measured and reported on the 24-hour Zeitgeber time scale, with ZT0 marked as "lights-
527 on" (at 06:00 PST) and ZT12 as "lights-off" (at 18:00 PST).

528 *Enriched environment*

529 For enriched-environment (EE) experimental conditions, animals were transferred from
530 their home cage in the standard environment to a larger cage in a different room
531 containing plastic and metal toys, tunnels, vertical scaffolds, and a running wheel. Mice
532 were placed in the EE with at least one cagemate and left to explore continuously for the
533 durations reported (i.e., for 30 minutes or 6 hours).

534 *Kainic-acid seizures*

535 Pharmacological seizures were induced using peritoneal injection of 15 mg/kg of kainic
536 acid (KA; Santa Cruz, #SC-200454) as described previously[36,66]. Seizure onset was
537 measured as the onset of rearing and accompanying bilateral forelimb clonus,
538 approximately corresponding to Racine stage 4[67]. Mice were sacrificed either 30 minutes
539 or 6 hours after seizure onset.

540 *snRNA-seq sample collection*

541 For sacrifice and sample collection, mice were deeply and rapidly anesthetized with
542 isoflurane in an induction chamber. Following induction, the brain was removed from the
543 skull into a dissection dish containing ice-cold dPBS (Gibco Cat. No. 14040133).
544 Hippocampus was rapidly extracted from one hemisphere, and the approximate CA1
545 area was microdissected using a microblade. Although the purpose of this
546 microdissection was to de-enrich samples of dentate granule cells, we still note that

547 these cells nevertheless comprise the 4th largest subclass in our dataset (**Fig. 1B**). The
548 dissected tissue sample was then placed in a microtube and flash-frozen. The other
549 hemisphere was placed in a cryomold as a whole, embedded in OCT compound, and
550 rapidly flash-frozen in isopentane chilled with dry ice. Left and right hemispheres were
551 alternated for the collection of CA1 and whole-hemisphere collection, across sexes and
552 conditions, to avoid any effects of lateralization (**Supp. Table 1**). Both samples from each
553 animal were stored at -70°C until use.

554 *Nucleus isolation and fixation*

555 Flash-frozen hippocampal dissectates were stored at -70°C until all experimental
556 samples had been collected. Before nucleus isolation, all buffers, tubes, and instruments
557 were pre-cooled on ice for 15-20 minutes before tissue was removed from -70°C.
558 Reusable instruments such as the Dounce tubes and pestles (Millipore cat. #D8938-
559 1SET) were rinsed with RNAse-free PBS and then with RNAse Away detergent before
560 being chilled on ice. All pipette tips (filtered tips only) and disposable tubes contacting
561 samples were RNAse-free. All buffers used during nucleus isolation contained
562 recombinant RNAsin to preserve RNA integrity (Promega, cat. #N2111), and actinomycin
563 D to prevent artifactual transcription stimulated by the isolation protocol (Tocris, cat.
564 #1229). Two main buffers were used for nucleus isolation: nucleus-isolation medium
565 (NIM) and NIM-Douce-pestle buffer. NIM buffer consisted of 250 mM sucrose, 25 mM
566 KCl, 5 mM MgCl2, 10 mM Tris-HCl (pH 7.4), 1 mM DTT, 0.2 U/uL RNAsin, 25 uM
567 actinomycin D, and 1 cOmplete protease inhibitor mini tablet (Roche cat.
568 #11836170001), dissolved in 10 mL of buffer. NIM-DP buffer consisted of 0.1% triton-X
569 100 detergent in NIM buffer.

570 To begin nucleus isolation, tissue samples were removed from -70°C and placed directly
571 on ice to thaw. No more than five samples underwent isolation at any one time in order
572 to minimize sample-handling time before fixation. First, 1 mL of NIM-DP buffer was
573 added to the sample storage microtube, and the sample was transferred to a 2 mL
574 Dounce tube using a 1000 uL pipette tip. Samples were homogenized using a Douce
575 pestle in 1 mL of NIM-DP buffer, first with 10 strokes of the loose pestle, and then 17
576 strokes of the tight pestle. Two sets of dounce tubes and pestles were used at a time,
577 and each was washed five times with PBS in-between samples. Dounced tissue
578 homogenates were then spun in a fixed-angle benchtop centrifuge at 800 x g for 8
579 minutes at 4°C. The supernatant was removed, and the nuclear pellet, clearly visible,

580 was resuspended thoroughly in 500 uL of NIM buffer using 30 strokes with a P200
581 pipette tip. Suspensions were then filtered through a 70 um filter before being spun at
582 200 x g for 10 min at 4°C in a swinging-bucket centrifuge. The supernatant was removed,
583 and nuclei pellets were resuspended in 187.5 uL of Parse Biosciences's "Resuspension
584 Buffer" and strained through a 20 um filter to begin Parse's Evercode Nuclei Fixation
585 protocol (version 1.1, kit chemistry v3). In total, samples/nuclei were suspended in
586 actinomycin D and kept on ice or in the pre-chilled centrifuge for the entirety of the
587 isolation protocol, which took approximately 1 hour before proceeding directly to the
588 Parse fixation protocol.

589 *snRNA-seq barcoding and library construction*

590 snRNA-seq library construction was performed using Parse Biosciences's Whole
591 Transcriptome v3 kit according to the manufacturer's protocol. Briefly, nuclei originating
592 from different samples are multiplexed and barcoded according to the SPLiT-pool
593 combinatorial barcoding method[27], wherein individual nuclei go through serial rounds of
594 PCR barcoding, pooling, and splitting amongst a 96-well plate containing well-specific
595 oligo barcodes. Split-pooling occurs in four serial barcoding rounds to ensure that each
596 nucleus has a unique combination of barcodes ligated. All samples were loaded and
597 barcoded together to avoid batch effects from separate library preparations. Libraries
598 were sequenced at the UCSD Institute for Genomic Medicine on an Illumina NovaSeq X
599 Plus using paired-end 100-bp reads. Sequencing was targeted at approximately 90,000
600 reads per nucleus, with a final average read depth of 66,702 reads per nucleus.

601 **Quantification and statistical analysis**

602 *Data preprocessing and quality control*

603 Nuclei quality control was performed as outlined in **Supplementary Figure 1**. Raw
604 nucleus x gene count matrices from demultiplexed samples were generated from the
605 FASTQ files using Parse Bioscience's Trailmaker software pipeline, version 1.4.1. A
606 "raw" Seurat object created by Trailmaker containing 110,728 nuclei, along with the
607 digital gene-count matrix, associated sample metadata, and DoubletFinder scores[68] was
608 downloaded and used to begin nuclei QC. Percent of reads mapping to mitochondrial
609 reads was calculated for each nucleus. Nuclei that did not meet the following criteria
610 were removed: transcript count (UMI) >= 1500; gene count >= 1500; and percent-
611 mitochondrial-read count <= 5%. After this filtering step, 108,748 nuclei remained. Allen
612 Brain Cell (ABC) taxonomic labels were assigned using the MapMyCells online tool. Next,

single-nucleus raw gene counts were transformed using Seurat's SCTransform function (v0.4.1), with the vars.to.regress argument set as the percent of reads mapping to mitochondrial genes (percent.mt) and SPLiT-Seq sublibrary. SCTransformation was computed across nuclei from all samples. (Note: Across-sample SCT-normalization, rather than within-sample normalization followed by integration was determined appropriate after normalizing, clustering, and visualizing UMAPs on a pilot sequencing run from this dataset, where we observed no batch effects due to sample or SPLiT-seq sublibrary). SCT-normalized counts were then used to perform principal component analysis (PCA), nearest-neighbor graph construction, initial Leiden cluster assignment, and uniform manifold approximation and projection (UMAP) embedding. This resulted in the segmentation of 108,748 nuclei into 47 Leiden clusters.

At this step, manual curation of 47 detected Leiden clusters was performed by experimenter J.O. cross-referencing plots and tables of UMI count, gene count, percent mitochondrial reads, doublet scores, and putative ABC cell type within each Leiden cluster. Based on these judgements, nuclei in 6 small Leiden clusters were removed because of low counts, high mitochondrial reads, high doublet scores, or the collision of many different putative ABC cell types. Finally, any nuclei with a DoubletFinder score < 0.02 were removed. After these quality-control steps, 93,066 nuclei remained. These again went through final PCA, Leiden clustering, and UMAP embedding to create the UMAP in **Figure 1**.

ABC taxon assignment stability

Stability of ABC taxonomy assignment for single nuclei was performed by comparing two separate runs of the curated data through the ABC atlas MapMyCells tool. The first run was performed using the native mouse transcriptome. The second run was performed after removing ARGs that had been ascertained in a published study of activity-dependent gene expression[2]. The stability of assignment was then determined by comparing taxon equality within the same barcode and visualized with Sankey flow diagrams (**Fig. 1E-H**).

Log2(FC) methods

Average log2(FC) expression values in **Figures 3** and **6** represent pseudobulk fold-change expression values calculated using DESeq2.

644 *Differential gene expression*

645 To identify differentially expressed genes (DEGs) across activity conditions, we
646 performed pseudobulk DGE analysis independently for each Subclass using DESeq2[69].
647 For each Subclass, nuclei were subset and grouped by their sample of origin.
648 Pseudobulk counts were aggregated at the sample level using Seurat's
649 AggregateExpression() function. Genes expressed in fewer than 1% of nuclei were
650 excluded. DESeq2 was then used to construct a DESeqDataSet with sample-level
651 counts and a design formula including activity condition (expression ~
652 activity_condition). Only condition contrasts meeting a minimum per-group nucleus
653 count threshold (n = 30 nuclei per condition) were retained for testing. Wald tests were
654 performed, and log2 fold changes were shrunken using the apeglm method. Genes with
655 absolute log2 fold change > 0.585 (corresponding to 1.5-fold change) and fdr < 0.05
656 were classified as differentially expressed. For analysis discovering DEGs between ZTs,
657 log2 fold change values were not shrunken. This was done for ZT analyses but not
658 activity analyses to minimize type II error rate; there are fewer biological replicates at
659 each ZT (**Supplementary Table 1**). Results were saved separately for each Subclass
660 and contrast.

661 *Hierarchical clustering*

662 For heatmap plots accompanied by a dendrogram, genes were ordered according to
663 hierarchical clustering of the Euclidean gene distances using the package
664 ComplexHeatmap[70]. In the heatmaps of **Figure 5**, genes were first clustered into 4 k-
665 means clusters, and only after were organized according to hierarchical methods within
666 each k-means cluster.

667 *ZT:Activity interaction testing*

668 To test for statistical interactions between the effect of ZT and the effect of activity on
669 gene expression, we used the linear formula

670 $$expression \sim ZT + activity + ZT{:}\,activity$$

671 to test for a significant ZT:Activity interaction term with DESeq2. Pseudobulk gene
672 counts were computed for each subclass separately. log2 fold changes were not
673 shrunken in this analysis in order to increase sensitivity of this test. For *a priori* gene sets,
674 multiple-hypothesis correction was performed by calculating the FDR among the *a priori*
675 gene set. For example, the FDR rates reported in **Figure 6A-D** were corrected for 15
676 multiple comparisons for the set of 15 IEGs. Only genes with an FDR < 0.05 were labeled
677 as significant DEGs.

678 *ERG vs LRG classification*

679 We used a similar method to a prior single-cell study to classify DEGs as mutually
680 exclusive early-response genes (ERGs) or late-response genes (LRGs)[10]. Classification
681 was performed separately for excitatory neurons, inhibitory neurons, and glial
682 Subclasses. First, DEGs for all Subclasses and contrasts (EE30m vs SE, EE6h vs SE)
683 were aggregated. Genes were provisionally labeled as ERG, LRG, or both based on
684 differentially expressed in EE 30 min or EE 6 hr. Genes initially labeled as "both" were
685 reclassified based on their peak fold-change timepoint. In cases where gene
686 classification differed across Subclasses, the modal classification was assigned. Final
687 classifications were saved for downstream analysis (**Figure 3**).

688 *Tau calculation*

689 We calculated a tau score for each gene, adapted from ref. [35], to discover and quantify
690 highly cell-type specific gene expression. For example, a gene with a tau score of 0
691 would have promiscuous expression among the cell types examined, whereas a gene
692 with a tau score approaching or greater than 1 would have highly cell-type specific
693 expression. For analyses on non-fold-change expression data among different cell types
694 (e.g. **Figure 5**), we directly applied the tau formula, in which tau was bounded by (0, 1):

695 $$\tau = \frac{1}{n-1}\sum_{i=1}^{n} \left(\frac{expression_i}{max(expression)}\right),$$

696 where n is the number of subclasses, and $expression_i$ represents the expression of the
697 gene in subclass i; in these analyses, our tau threshold was set at 0.75 due to the index
698 being bounded by (0, 1). For analyses on fold-change expression where expression
699 values can be negative, the tau score was bounded by (0, ∞); for these analyses, our tau
700 threshold was set higher at 0.8. In practice, tau scores above 0.75 were observed to be
701 highly specific to one or a small number of subclasses.

702 *Defining active cells*

703 In order to determine the number of cells activated within a given condition, it was
704 determined whether cells expressed the IEGs above a certain threshold: The IEG list was
705 defined *a priori* based on the following 15 canonical IEGs: *Arc, Btg2, Dusp1, Dusp5,*
706 *Egr1, Egr2, Egr3, Egr4, Fos, Fosb, Fosl2, Junb, Npas4, Nr4a1,* and *Nr4a3*. The induction
707 threshold was determined for each gene individually, and was defined as the 90th
708 percentile of expression in SE cells of the CA1 subclass. Thus, for each gene in the gene
709 list, a binary classification was assigned as either induced or not-induced based on
710 whether or not it surpassed the expression threshold (**Fig. 4A**). Finally, a cell was defined
711 as "active" if it induced at least 20% of the genes (i.e., 3 or more) in the activity-regulated-
712 gene list.

713 Data and code availability

714 Fastq files for sequenced reads will be publicly deposited in the GEO database.
715 Metadata for biological replicates can be downloaded from the GEO database or
716 https://github.com/Bloodgood-Lab/Olmstead-2025-preprint. We used the Trailmaker
717 pipeline running split-pipe v1.4.1 through Parse Biosciences' web portal for creation of
718 the cell-count matrix and unprocessed Seurat object, which will be publicly deposited in
719 the GEO database. All the code and package versions to reproduce this manuscript are
720 publicly available at https://github.com/Bloodgood-Lab/Olmstead-2025-preprint.

References

1. Greenberg, M. E. & Ziff, E. B. Stimulation of 3T3 cells induces transcription of the c-fos proto-oncogene. *Nature* **311**, 433–438 (1984).
2. Tyssowski, K. M. *et al.* Different Neuronal Activity Patterns Induce Different Gene Expression Programs. *Neuron* **98**, 530-546.e11 (2018).
3. Guzowski, J. F., McNaughton, B. L., Barnes, C. A. & Worley, P. F. Environment-specific expression of the immediate-early gene Arc in hippocampal neuronal ensembles. *Nat Neurosci* **2**, 1120–1124 (1999).
4. Tullai, J. W. *et al.* Immediate-Early and Delayed Primary Response Genes Are Distinct in Function and Genomic Architecture*. *Journal of Biological Chemistry* **282**, 23981–23995 (2007).
5. Lituma, P. J., Singer, R. H., Das, S. & Castillo, P. E. Real-time imaging of Arc/Arg3.1 transcription ex vivo reveals input-specific immediate early gene dynamics. *Proceedings of the National Academy of Sciences* **119**, e2123373119 (2022).
6. Akiki, R. M. *et al.* A long noncoding eRNA forms R-loops to shape emotional experience–induced behavioral adaptation. *Science* **386**, 1282–1289 (2024).
7. Yao, Z. *et al.* A high-resolution transcriptomic and spatial atlas of cell types in the whole mouse brain. *Nature* **624**, 317–332 (2023).
8. Langlieb, J. *et al.* The molecular cytoarchitecture of the adult mouse brain. *Nature* **624**, 333–342 (2023).
9. Lacar, B. *et al.* Nuclear RNA-seq of single neurons reveals molecular signatures of activation. *Nat Commun* **7**, 11022 (2016).
10. Hrvatin, S. *et al.* Single-cell analysis of experience-dependent transcriptomic states in the mouse visual cortex. *Nat Neurosci* **21**, 120–129 (2018).
11. Jarrard, L. E. On the role of the hippocampus in learning and memory in the rat. *Behavioral and Neural Biology* **60**, 9–26 (1993).
12. O'Keefe, J. & Dostrovsky, J. The hippocampus as a spatial map. Preliminary evidence from unit activity in the freely-moving rat. *Brain Research* **34**, 171–175 (1971).
13. Nádasdy, Z., Hirase, H., Czurkó, A., Csicsvari, J. & Buzsáki, G. Replay and Time Compression of Recurring Spike Sequences in the Hippocampus. *J. Neurosci.* **19**, 9497–9507 (1999).
14. Buzsáki, G. Hippocampal sharp wave-ripple: A cognitive biomarker for episodic memory and planning. *Hippocampus* **25**, 1073–1188 (2015).
15. Joo, H. R. & Frank, L. M. The hippocampal sharp wave–ripple in memory retrieval for immediate use and consolidation. *Nat Rev Neurosci* **19**, 744–757 (2018).

16. Carr, M. F., Jadhav, S. P. & Frank, L. M. Hippocampal replay in the awake state: a potential substrate for memory consolidation and retrieval. *Nat Neurosci* **14**, 147–153 (2011).

17. Pfeiffer, B. E. The content of hippocampal “replay”. *Hippocampus* **30**, 6–18 (2020).

18. Bellfy, L. *et al.* The clock gene Per1 may exert diurnal control over hippocampal memory consolidation. *Neuropsychopharmacol.* **48**, 1789–1797 (2023).

19. Kwapis, J. L. *et al.* Epigenetic regulation of the circadian gene Per1 contributes to age-related changes in hippocampal memory. *Nat Commun* **9**, 3323 (2018).

20. Harvey, J. R. M., Plante, A. E. & Meredith, A. L. Ion Channels Controlling Circadian Rhythms in Suprachiasmatic Nucleus Excitability. *Physiological Reviews* **100**, 1415–1454 (2020).

21. Gonzalez, J. C. *et al.* Circadian regulation of dentate gyrus excitability mediated by G-protein signaling. *Cell Reports* **42**, 112039 (2023).

22. Flourakis, M. *et al.* A Conserved Bicycle Model for Circadian Clock Control of Membrane Excitability. *Cell* **162**, 836–848 (2015).

23. Birnie, M. T. *et al.* Circadian regulation of hippocampal function is disrupted with corticosteroid treatment. *Proceedings of the National Academy of Sciences* **120**, e2211996120 (2023).

24. Gerstner, J. R. *et al.* BMAL1 controls the diurnal rhythm and set point for electrical seizure threshold in mice. *Front. Syst. Neurosci.* **8**, (2014).

25. Karoly, P. J. *et al.* Circadian and circaseptan rhythms in human epilepsy: a retrospective cohort study. *The Lancet Neurology* **17**, 977–985 (2018).

26. Rawashdeh, O. *et al.* PERIOD1 coordinates hippocampal rhythms and memory processing with daytime. *Hippocampus* **24**, 712–723 (2014).

27. Rosenberg, A. B. *et al.* Single-cell profiling of the developing mouse brain and spinal cord with split-pool barcoding. *Science* **360**, 176–182 (2018).

28. Fernandez-Albert, J. *et al.* Immediate and deferred epigenomic signatures of in vivo neuronal activation in mouse hippocampus. *Nat Neurosci* **22**, 1718–1730 (2019).

29. Traunmüller, L. *et al.* Novel environment exposure drives temporally defined and region-specific chromatin accessibility and gene expression changes in the hippocampus. *Nat Commun* **16**, 7787 (2025).

30. Johnson, A., Varberg, Z., Benhardus, J., Maahs, A. & Schrater, P. The hippocampus and exploration: dynamically evolving behavior and neural representations. *Front. Hum. Neurosci.* **6**, (2012).

31. Diamantaki, M., Frey, M., Berens, P., Preston-Ferrer, P. & Burgalossi, A. Sparse activity of identified dentate granule cells during spatial exploration. *eLife* **5**, e20252 (2016).

32. Chavlis, S., Petrantonakis, P. C. & Poirazi, P. Dendrites of dentate gyrus granule cells contribute to pattern separation by controlling sparsity: DENDRITIC ROLE IN PATTERN SEPARATION. *Hippocampus* **27**, 89–110 (2017).

33. Lee, J. Q. *et al.* Sparsity of Population Activity in the Hippocampus Is Task-Invariant Across the Trisynaptic Circuit and Dorsoventral Axis. *Hippocampus* **35**, e23651 (2025).

34. Borzello, M. *et al.* Assessments of dentate gyrus function: discoveries and debates. *Nat. Rev. Neurosci.* **24**, 502–517 (2023).

35. Yanai, I. *et al.* Genome-wide midrange transcription profiles reveal expression level relationships in human tissue specification. *Bioinformatics* **21**, 650–659 (2005).

36. Pollina, E. A. *et al.* A NPAS4–NuA4 complex couples synaptic activity to DNA repair. *Nature* 1–10 (2023) doi:10.1038/s41586-023-05711-7.

37. Yao, Z. *et al.* A transcriptomic and epigenomic cell atlas of the mouse primary motor cortex. *Nature* **598**, 103–110 (2021).

38. van Strien, N. M., Cappaert, N. L. M. & Witter, M. P. The anatomy of memory: an interactive overview of the parahippocampal–hippocampal network. *Nat Rev Neurosci* **10**, 272–282 (2009).

39. Rolotti, S. V., Blockus, H., Sparks, F. T., Priestley, J. B. & Losonczy, A. Reorganization of CA1 dendritic dynamics by hippocampal sharp-wave ripples during learning. *Neuron* **110**, 977-991.e4 (2022).

40. Foster, D. j., Morris, R. g. m. & Dayan, P. A model of hippocampally dependent navigation, using the temporal difference learning rule. *Hippocampus* **10**, 1–16 (2000).

41. Dragoi, G. & Tonegawa, S. Preplay of future place cell sequences by hippocampal cellular assemblies. *Nature* **469**, 397–401 (2011).

42. Hor, C. N. *et al.* Sleep–wake-driven and circadian contributions to daily rhythms in gene expression and chromatin accessibility in the murine cortex. *Proc. Natl. Acad. Sci. U.S.A.* **116**, 25773–25783 (2019).

43. Reick, M., Garcia, J. A., Dudley, C. & McKnight, S. L. NPAS2: An Analog of Clock Operative in the Mammalian Forebrain. *Science* **293**, 506–509 (2001).

44. Wang, L. M. C. *et al.* Expression of the Circadian Clock Gene Period2 in the Hippocampus: Possible Implications for Synaptic Plasticity and Learned Behaviour. *ASN Neuro* **1**, AN20090020 (2009).

45. Jilg, A. *et al.* Temporal dynamics of mouse hippocampal clock gene expression support memory processing. *Hippocampus* **20**, 377–388 (2010).

833 46. Moriya, S., Tahara, Y., Sasaki, H., Ishigooka, J. & Shibata, S. Housing under
834 abnormal light–dark cycles attenuates day/night expression rhythms of the clock
835 genes Per1, Per2, and Bmal1 in the amygdala and hippocampus of mice.
836 *Neuroscience Research* **99**, 16–21 (2015).

837 47. Bering, T., Blancas-Velazquez, A. S. & Rath, M. F. Circadian Clock Genes Are
838 Regulated by Rhythmic Corticosterone at Physiological Levels in the Rat
839 Hippocampus. *Neuroendocrinology* **113**, 1076–1090 (2023).

840 48. Chiou, Y.-Y. *et al.* Mammalian Period represses and de-represses transcription by
841 displacing CLOCK–BMAL1 from promoters in a Cryptochrome-dependent
842 manner. *Proc. Natl. Acad. Sci. U.S.A.* **113**, (2016).

843 49. Eckel-Mahan, K. L. *et al.* Circadian oscillation of hippocampal MAPK activity and
844 cAMP: implications for memory persistence. *Nat Neurosci* **11**, 1074–1082 (2008).

845 50. Cirelli, C. & Tononi, G. Gene expression in the brain across the sleep–waking
846 cycle1. *Brain Research* **885**, 303–321 (2000).

847 51. Phan, T. H., Chan, G. C.-K., Sindreu, C. B., Eckel-Mahan, K. L. & Storm, D. R. The
848 Diurnal Oscillation of MAP (Mitogen-Activated Protein) Kinase and Adenylyl
849 Cyclase Activities in the Hippocampus Depends on the Suprachiasmatic Nucleus.
850 *J. Neurosci.* **31**, 10640–10647 (2011).

851 52. Squair, J. W. *et al.* Confronting false discoveries in single-cell differential
852 expression. *Nat Commun* **12**, 5692 (2021).

853 53. Zimmerman, K. D., Espeland, M. A. & Langefeld, C. D. A practical solution to
854 pseudoreplication bias in single-cell studies. *Nat Commun* **12**, 738 (2021).

855 54. Denny, C. A. *et al.* Hippocampal Memory Traces Are Differentially Modulated by
856 Experience, Time, and Adult Neurogenesis. *Neuron* **83**, 189–201 (2014).

857 55. Sun, X. *et al.* Functionally Distinct Neuronal Ensembles within the Memory
858 Engram. *Cell* **181**, 410-423.e17 (2020).

859 56. Guenthner, C. J., Miyamichi, K., Yang, H. H., Heller, H. C. & Luo, L. Permanent
860 Genetic Access to Transiently Active Neurons via TRAP: Targeted Recombination
861 in Active Populations. *Neuron* **78**, 773–784 (2013).

862 57. Sørensen, A. T. *et al.* A robust activity marking system for exploring active
863 neuronal ensembles. *eLife* **5**, e13918 (2016).

864 58. Riggle, J. P. *et al.* Spontaneous Recovery of Circadian Organization in Mice
865 Lacking a Core Component of the Molecular Clockwork. *J Biol Rhythms* **37**, 94–
866 109 (2022).

867 59. Tunnacliffe, E. & Chubb, J. R. What Is a Transcriptional Burst? *Trends in Genetics*
868 **36**, 288–297 (2020).

869 60. Corrigan, A. M. & Chubb, J. R. Regulation of Transcriptional Bursting by a
870 Naturally Oscillating Signal. *Current Biology* **24**, 205–211 (2014).

871 61. Coulon, A., Chow, C. C., Singer, R. H. & Larson, D. R. Eukaryotic transcriptional
872 dynamics: from single molecules to cell populations. *Nat Rev Genet* **14**,
873 10.1038/nrg3484 (2013).

874 62. Chen, L.-F. *et al.* Enhancer Histone Acetylation Modulates Transcriptional
875 Bursting Dynamics of Neuronal Activity-Inducible Genes. *Cell Reports* **26**, 1174-
876 1188.e5 (2019).

877 63. Luo, J., Phan, T. X., Yang, Y., Garelick, M. G. & Storm, D. R. Increases in cAMP,
878 MAPK Activity, and CREB Phosphorylation during REM Sleep: Implications for
879 REM Sleep and Memory Consolidation. *J. Neurosci.* **33**, 6460–6468 (2013).

880 64. Saraf, A., Luo, J., Morris, D. R. & Storm, D. R. Phosphorylation of Eukaryotic
881 Translation Initiation Factor 4E and Eukaryotic Translation Initiation Factor 4E-
882 binding Protein (4EBP) and Their Upstream Signaling Components Undergo
883 Diurnal Oscillation in the Mouse Hippocampus. *Journal of Biological Chemistry*
884 **289**, 20129–20138 (2014).

885 65. Rönnbäck, A., Dahlqvist, P., Bergström, S.-A. & Olsson, T. Diurnal effects of
886 enriched environment on immediate early gene expression in the rat brain. *Brain*
887 *Research* **1046**, 137–144 (2005).

888 66. Bosco, D. B. *et al.* RNAseq analysis of hippocampal microglia after kainic acid-
889 induced seizures. *Mol Brain* **11**, 34 (2018).

890 67. Racine, R. J. Modification of seizure activity by electrical stimulation: II. Motor
891 seizure. *Electroencephalography and Clinical Neurophysiology* **32**, 281–294
892 (1972).

893 68. McGinnis, C. S., Murrow, L. M. & Gartner, Z. J. DoubletFinder: Doublet Detection
894 in Single-Cell RNA Sequencing Data Using Artificial Nearest Neighbors. *Cell*
895 *Systems* **8**, 329-337.e4 (2019).

896 69. Love, M. I., Huber, W. & Anders, S. Moderated estimation of fold change and
897 dispersion for RNA-seq data with DESeq2. *Genome Biology* **15**, 550 (2014).

898 70. Gu, Z., Eils, R. & Schlesner, M. Complex heatmaps reveal patterns and
899 correlations in multidimensional genomic data. *Bioinformatics* **32**, 2847–2849
900 (2016).

Supplementary Figure 1

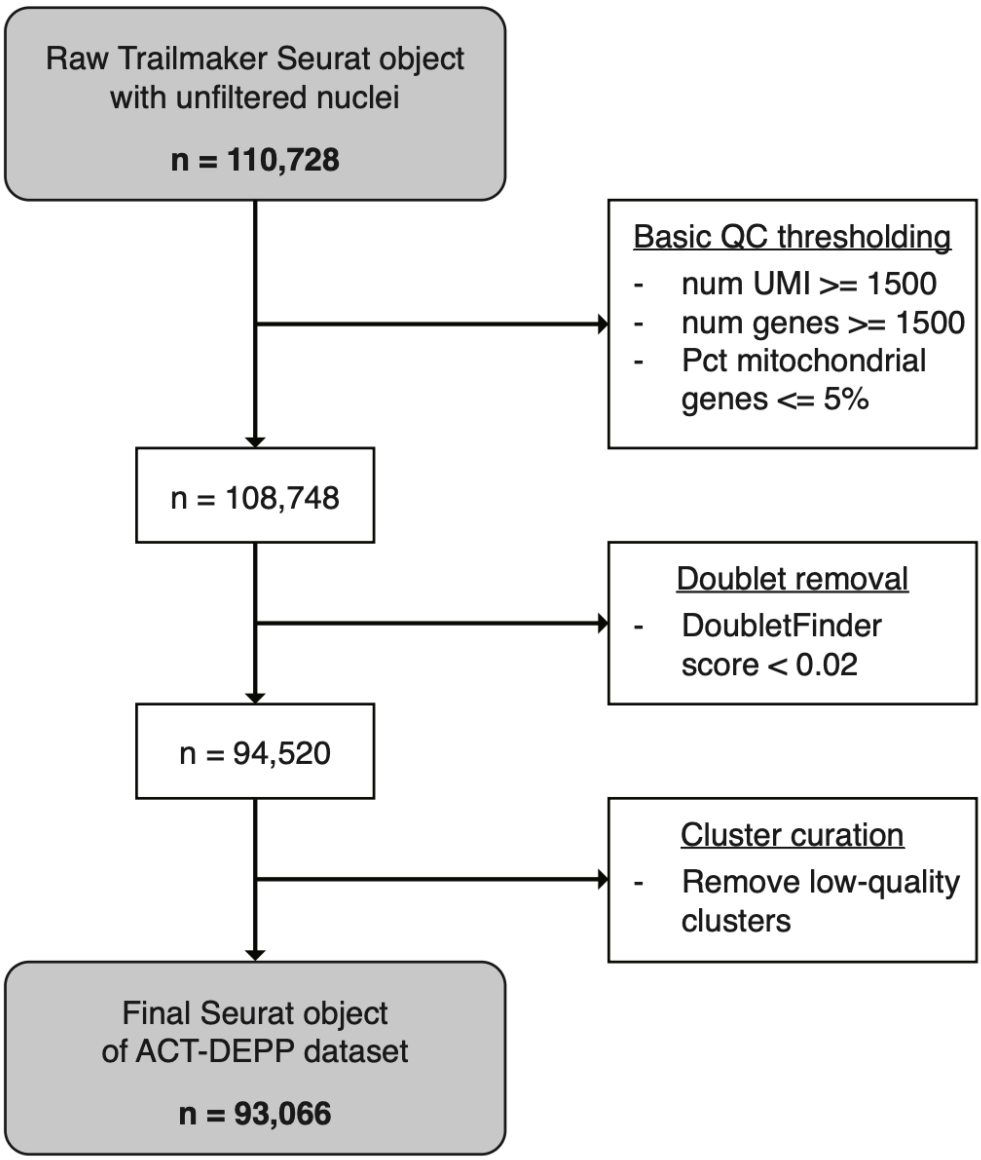

Supplementary Figure 1. Quality control of single-nuclei dataset.
The initial unfiltered Seurat object was downloaded from Parse Biosciences' Trailmaker pipeline. Nuclei underwent QC thresholding, doublet rejection, and preliminary clustering to arrive at the final dataset of 93,066 nuclei.

Supplementary Figure 2

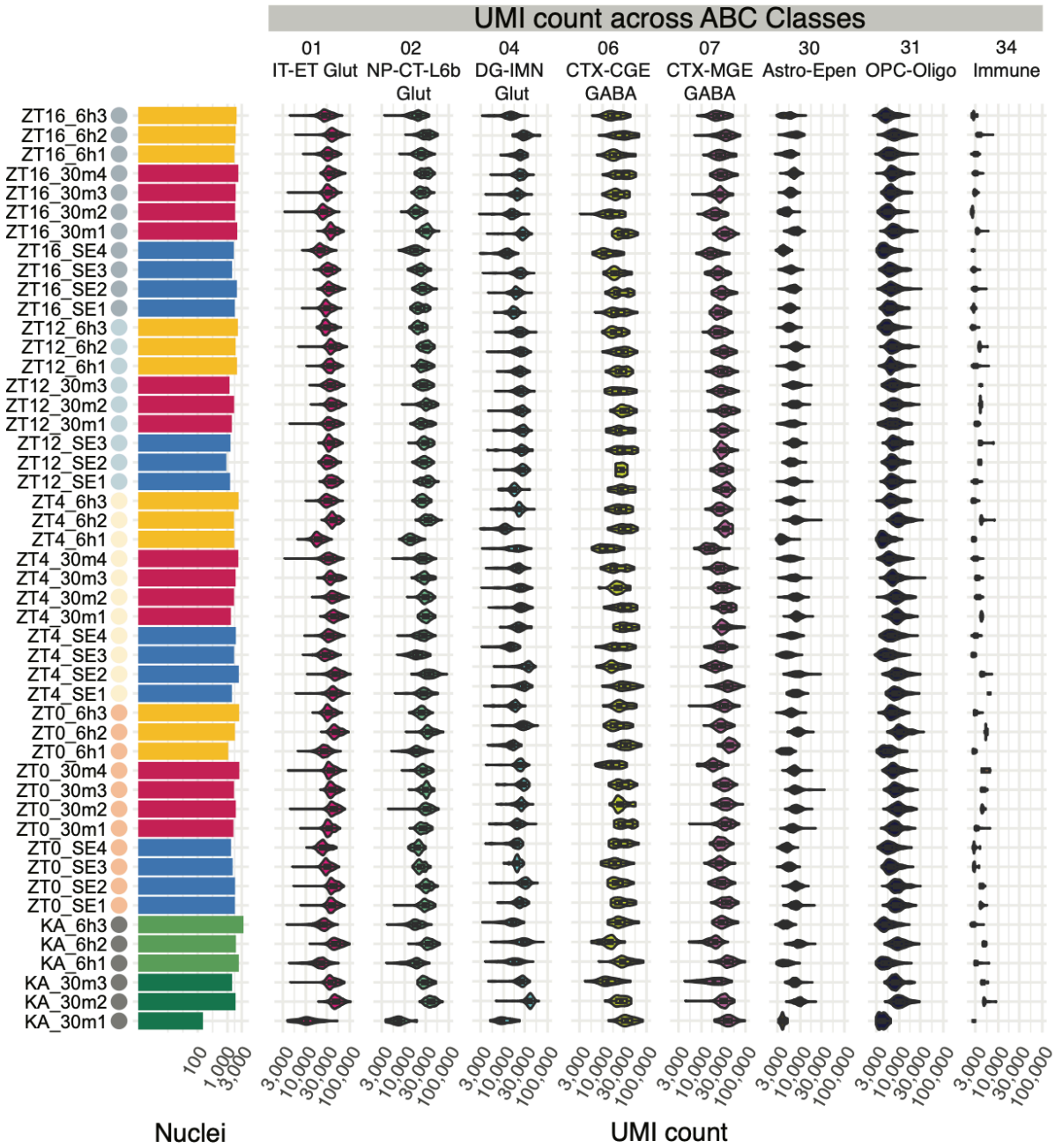

Supplementary Figure 2. UMI counts across major cell types.
Nuclei (left) and unique molecular identifier (UMI) counts (right) across major cell types in all biological replicates of the ACT-DEPP dataset. Colored dots on the left correspond to ZT times tested.

Supplementary Figure 3

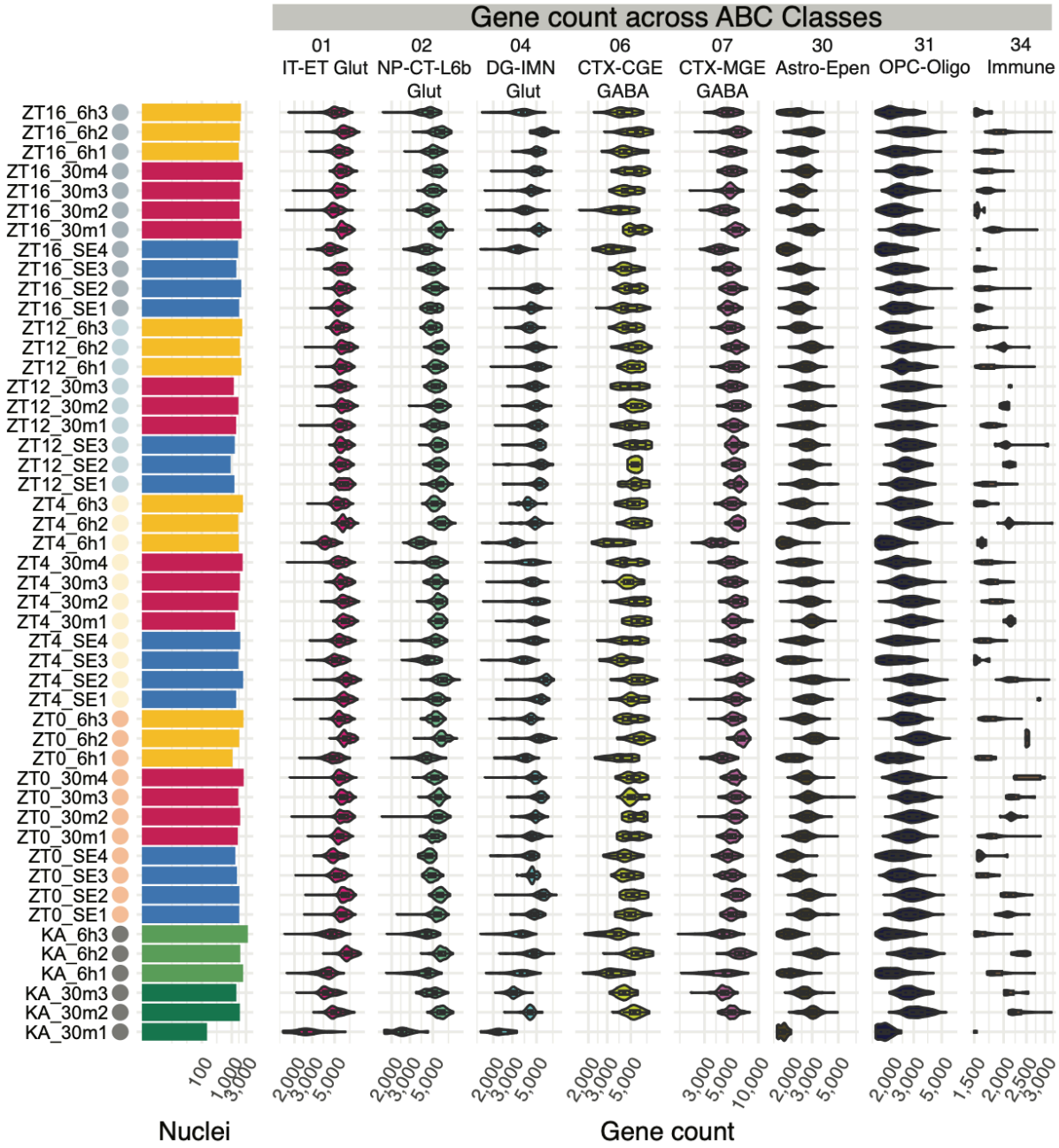

Supplementary Figure 3. Gene counts across major cell types.
Nuclei (left) and gene counts (right) across major cell types in all biological replicates of the ACT-DEPP dataset. Colored dots on the left correspond to ZT times tested.

Factor design in ACT-DEPP dataset									
				Sex		Hemisphere		Nuclei	
		Age ± sd	Replicates	M	F	R	L	Total	Average
SE	ZT0	30.0 ± 0.0	4	2	2	2	2	6,912	1,728
	ZT4	28.5 ± 0.6	4	2	2	2	2	8,424	2,106
	ZT12	30.0 ± 0.0	3	2	1	2	1	3,656	1,219
	ZT16	28.0 ± 0.0	4	2	2	2	2	8,016	2,004
	n_{total}		15	8	7	8	7	27,008	7,057
EE30m	ZT0	30.0 ± 0.0	4	2	2	2	2	8,091	2,023
	ZT4	28.5 ± 0.6	4	2	2	2	2	7,596	1,899
	ZT12	32.0 ± 0.0	3	2	1	2	1	4,497	1,499
	ZT16	28.5 ± 0.6	4	2	2	2	2	9,179	2,295
	n_{total}		15	8	7	8	7	29,363	7,716
EE6h	ZT0	29.0 ± 0.0	3	1	2	3	0	5,983	1,994
	ZT4	28.0 ± 0.0	3	1	2	2	1	6,114	2,038
	ZT12	31.0 ± 0.0	3	1	2	1	2	6,685	2,228
	ZT16	32.0 ± 0.0	3	1	2	2	1	5,946	1,982
	n_{total}		12	4	8	8	4	24,728	8,243
KA30m	—	29.0 ± 0.0	3	1	2	1	2	3,744	1,248
KA6h	—	29.0 ± 0.0	3	1	2	1	2	8,223	2,741
$n_{ACT\text{-}DEPP}$			48	22	26	26	22	93,066	

Supplementary Table 1. Factor design in the ACT-DEPP dataset.